

Primordial Monopoles and Strings, Inflation, and Gravity Waves

Joydeep Chakraborty,¹ George Lazarides,² Rinku Maji,¹ Qaisar Shafi³

¹*Indian Institute of Technology Kanpur, Kalyanpur, Kanpur 208016, Uttar Pradesh, INDIA*

²*School of Electrical and Computer Engineering, Faculty of Engineering, Aristotle University of Thessaloniki, Thessaloniki 54124, Greece*

³*Bartol Research Institute, Department of Physics and Astronomy, University of Delaware, Newark, DE 19716, USA*

ABSTRACT: We consider magnetic monopoles and strings that appear in non-supersymmetric $SO(10)$ and E_6 grand unified models paying attention to gauge coupling unification and proton decay in a variety of symmetry breaking schemes. The dimensionless string tension parameter $G\mu$ spans the range $10^{-6} - 10^{-30}$, where G is Newton's constant and μ is the string tension. We show how intermediate scale monopoles with mass $\sim 10^{13} - 10^{14}$ GeV and flux $\lesssim 2.8 \times 10^{-16}$ cm⁻²s⁻¹sr⁻¹, and cosmic strings with $G\mu \sim 10^{-11} - 10^{-10}$ survive inflation and are present in the universe at an observable level. We estimate the gravity wave spectrum emitted from cosmic strings taking into account inflation driven by a Coleman-Weinberg potential. The tensor-to-scalar ratio r lies between 0.06 and 0.003 depending on the details of the inflationary scenario.

Contents

1	Introduction	1
2	Renormalization Group Equations (RGEs) for Gauge Couplings	3
3	Symmetry Breaking and Topological Defects	5
3.1	$SO(10)$ without Strings or Necklaces	6
3.2	$SO(10)$ with Strings and Necklaces	7
3.3	E_6 without Strings	8
3.4	E_6 with Strings	9
4	Unification with Threshold Corrections and Proton Decay	10
5	Inflation with Coleman-Weinberg Potential	12
6	Phase Transitions and Formation of Topological Defects	17
7	Intermediate Mass Monopoles	18
8	Intermediate Scale Strings and Gravity Waves	21
9	Phase Transition after Inflation	24
10	Conclusions	26
11	Acknowledgment	27
	Appendix: RGEs for the Two Breaking Chains of $SO(10)$	27

1 Introduction

Grand Unified Theories (GUTs) such as $SU(5)$, $SO(10)$ (more precisely $Spin(10)$), and E_6 predict the existence of a topologically stable [1, 2] superheavy magnetic monopole of mass $\sim M_X/\alpha_X$, where α_X denotes the gauge fine structure constant at the unified scale $M_X \sim 10^{16}$ GeV. This monopole carries a single quantum of Dirac magnetic charge as well as color magnetic charge, which is related to the fact that the unbroken subgroup is $SU(3)_C \otimes U(1)_{em}/Z_3$ [3, 4]. In non-supersymmetric $SO(10)$ and E_6 models, the symmetry breaking to the Standard Model (SM) gauge group proceeds via one or more intermediate steps which has important consequences for monopole masses and charges. For instance, the breaking of $SO(10)$ via

$SU(2)_L \otimes SU(2)_R \otimes SU(4)_C$ [5] yields intermediate mass monopoles that carry two quanta of Dirac magnetic charge [6, 7]. This is an important difference from $SU(5)$ because the intermediate mass monopole in $SO(10)$ with two units of magnetic charge is a few orders of magnitude lighter than the $SO(10)$ monopole carrying one unit of charge which is again superheavy. Clearly, this cannot happen in $SU(5)$. Similarly, in E_6 if the breaking occurs via $SU(3)^3$ we find intermediate mass monopoles carrying three quanta of Dirac charge [7–12]. The discovery of primordial monopoles with intermediate mass scales would have profound consequences for particle physics and cosmology.

The discovery of topologically stable intermediate scale cosmic strings would also have critical ramifications for the physics of the early universe and particle physics extensions of the SM. The first and most well known example of topologically stable cosmic strings appearing in GUTs is provided by $SO(10)$ [13]. If the breaking of $SO(10)$ to the SM gauge group is carried out using scalar vacuum expectation values (VEVs) in the tensor representations, a Z_2 symmetry remains unbroken which implies the presence of topologically stable cosmic strings. Note that a direct breaking of $SO(10)$ to the SM gauge group would yield GUT scale cosmic strings which is excluded by the WMAP and Planck satellite data [14, 15] as well as the limits from pulsar timing arrays (PTA) [16–20]. (For recent developments see Refs. [21–24]). In other words, we expect the breaking to proceed via intermediate steps which is favored for non-supersymmetric $SO(10)$ for other phenomenological reasons. Thus, we are interested in exploring intermediate scale cosmic strings that appear in $SO(10)$ and E_6 models.

In this paper, we consider two symmetry breaking chains for each of the non-supersymmetric $SO(10)$ and E_6 GUTs with two intermediate steps. Superheavy magnetic monopoles with one unit of Dirac magnetic charge are predicted in all cases along with intermediate scale monopoles with two units or three units of Dirac magnetic charge in $SO(10)$ or E_6 , respectively. Intermediate scale cosmic strings appear in one of the $SO(10)$ and one of the E_6 models. The GUT and intermediate scales are determined so that all the low energy data and the constraint from proton decay are satisfied. We merge these models with inflation driven by a Coleman-Weinberg potential of a scalar gauge singlet [25, 26] and further restrict the model parameters by requiring that the data for all the inflationary observables are reproduced. Studying carefully the phase transitions during which the GUT and intermediate symmetry breakings take place, we discuss the generation and subsequent evolution of magnetic monopoles and cosmic strings as well as the emission of gravity waves from the decaying strings.

The paper is organized as follows. In Sec. 2, we summarize the important features of the renormalization group equations (RGEs) for the gauge coupling constants. This section includes a brief discussion on beta functions, Abelian mixing, and the matching conditions along with the threshold corrections. In Sec. 3, we describe the details of the symmetry breaking chains for the GUT models and the emergence of topological defects at different stages of symmetry breaking. We also present in this section and in the Appendix the beta coefficients associated with each of these breaking scenarios. In Sec. 4, we perform a goodness of fit test to estimate the solutions of RGEs for each case in terms of the unification and intermediate scales which are compatible with the low energy data and the proton lifetime constraint. We discuss in

Sec. 5 the inflationary dynamics with a Coleman-Weinberg potential where the inflaton is a scalar GUT singlet [25], and determine the values of the model parameters that yield successful inflation. In Sec. 6, we analyze the phase transitions during inflation which are associated with the unification and the intermediate scales, and in Sec. 7, the monopole production during the first intermediate phase transition is discussed. The generation of cosmic strings during the second intermediate phase transition and their subsequent evolution is presented in Sec. 8 together with the emission of gravity waves. In Sec. 9, we extend our analysis to the case that the second intermediate phase transition takes place after the end of inflation, i.e. either during inflaton oscillations or after reheating. In Sec. 10, we summarize our conclusions.

2 Renormalization Group Equations (RGEs) for Gauge Couplings

The RGEs for the gauge couplings g_i ($i = 1, 2, \dots, n$) corresponding to a generic product gauge group of the form $\mathcal{G} \equiv \mathcal{G}_1 \otimes \mathcal{G}_2 \otimes \dots \otimes \mathcal{G}_n$ can be written as (up to two loop) [27–33]:

$$\mu \frac{dg_i}{d\mu} = \frac{1}{16\pi^2} b_i g_i^3 + \frac{1}{(16\pi^2)^2} \sum_{j=1}^n b_{ij} g_i^3 g_j^2, \quad (2.1)$$

where μ is the renormalization scale parameter (not to be confused with the string tension) and

$$\begin{aligned} b_i &= \frac{4\kappa}{3} T(F_i) D_{F_i} + \frac{1}{3} \eta T(S_i) D_{S_i} - \frac{11}{3} C_2(\mathcal{G}_i), \\ b_{ij} &= \left[\left(\frac{20}{3} C_2(\mathcal{G}_i) + 4C_2(F_i) \right) \kappa T(F_i) D_{F_i} \right. \\ &\quad \left. + \left(\frac{2}{3} C_2(\mathcal{G}_i) + 4C_2(S_i) \right) \eta T(S_i) D_{S_i} - \frac{34}{3} (C_2(\mathcal{G}_i))^2 \right] \delta_{ij} \\ &\quad + 4 (\kappa C_2(F_j) T(F_i) D_{F_i} + \eta C_2(S_j) T(S_i) D_{S_i}) \end{aligned} \quad (2.2)$$

are the one- and two-loop β -coefficients respectively with $\kappa = 1$ ($1/2$) for Dirac (Weyl) fermions and $\eta = 1$ ($1/2$) for complex (real) scalars. F_i (S_i) denote the fermion (scalar) representations transforming under \mathcal{G}_i , $T(R_i)$ is the normalization of the representation R_i ¹, $C_2(\mathcal{G}_i)$ is the quadratic Casimir operator for the group \mathcal{G}_i , and $C_2(R_i)$ is the quadratic Casimir operator for the representation R_i . Also, $D_{R_i} = \prod_{j \neq i} D(R_j)$ with $D(R_i)$ being the dimension of the i th representation in the multiplet $R = (R_1, R_2, \dots, R_n)$.

The multiple occurrence of Abelian groups leads to the mixing of their gauge couplings even at the one-loop level [34–41]. In this case, instead of treating the individual evolution of each Abelian gauge coupling, we need to consider the complete Abelian gauge coupling matrix,

¹It is defined as $\text{Tr}(T^a T^b) = T(R) \delta^{ab} = 2\ell_R \delta^{ab}$, with T^a being the generators of the group, ℓ_R is the Dynkin index corresponding to the representation R , and $a, b = 1, 2, \dots, d_{\mathcal{G}}$, where $d_{\mathcal{G}}$ is the dimension of the group.

e.g. for two Abelian gauge groups $U(1)_1 \otimes U(1)_2$ we should consider the following matrix

$$g = \begin{pmatrix} g_{11} & g_{12} \\ g_{21} & g_{22} \end{pmatrix}, \quad (2.3)$$

and the RGEs of the individual matrix elements g_{cb} with $c, b = 1, 2$ can be expressed as:

$$\mu \frac{dg_{cb}}{d\mu} = \beta_{ab} g_{ca}, \quad (2.4)$$

where

$$\beta_{ab} = \frac{1}{(4\pi)^2} g_{ia} \left(\beta_{ij}^{1L} + \frac{1}{(4\pi)^2} \beta_{ij}^{2L} \right) g_{jb}. \quad (2.5)$$

The one-loop beta coefficients are

$$\beta_{ij}^{1L} = \tilde{b}_{ij} = \frac{4}{3} \kappa q_i^F q_j^F D(F) + \frac{1}{3} \eta q_i^S q_j^S D(S), \quad (2.6)$$

where $q_i^{F(S)}$ is the Abelian $U(1)_i$ charge of the fermion (scalar) multiplet F (S). Similarly, the two-loop beta coefficients are

$$\beta_{ij}^{2L} = \tilde{b}_{ij,kl} g_{km} g_{lm} = \tilde{b}_{ij,kl} (g_{k1} g_{l1} + g_{k2} g_{l2}), \quad (2.7)$$

with

$$\tilde{b}_{ij,kl} = 4 \left(\kappa q_i^F q_j^F q_k^F q_l^F D(F) + \eta q_i^S q_j^S q_k^S q_l^S D(S) \right). \quad (2.8)$$

It is interesting to note that at the two-loop level, the RGEs of the non-Abelian gauge couplings g_r receive additional contributions due to the Abelian gauge coupling mixing. The additional contributions are of the following forms:

$$\mu \frac{dg_r}{d\mu} \supset \frac{1}{(4\pi)^4} b_{ij,r} g_r^3 g_{ik} g_{jk} \quad \text{and} \quad \beta_{ij}^{2\text{loop}} \supset \tilde{b}_{ij,r} g_r^2, \quad (2.9)$$

where

$$\begin{aligned} b_{ij,r} &= 4 \left(\kappa q_i^F q_j^F T(F_r) D_{F_r} + \eta q_i^S q_j^S T(S_r) D_{S_r} \right), \\ \tilde{b}_{ij,r} &= 4 \left(\kappa q_i^F q_j^F C_2(F_r) + \eta q_i^S q_j^S C_2(S_r) \right). \end{aligned} \quad (2.10)$$

If a non-Abelian parent symmetry \mathcal{G}_P is spontaneously broken to another non-Abelian daughter symmetry \mathcal{G}_D , the appropriate matching condition at the scale μ along with the one-loop threshold correction $\Lambda_D(\mu)$ is given as [38, 42–46]:

$$\frac{1}{\alpha_D(\mu)} - \frac{C_2(\mathcal{G}_D)}{12\pi} = \left(\frac{1}{\alpha_P(\mu)} - \frac{C_2(\mathcal{G}_P)}{12\pi} \right) - \frac{\Lambda_D(\mu)}{12\pi}, \quad (2.11)$$

where

$$\Lambda_D(\mu) = -21 \operatorname{Tr}(t_{DV}^2 \ln \frac{M_V}{\mu}) + 2 \eta \operatorname{Tr}(t_{DS}^2 \ln \frac{M_S}{\mu}) + 8 \kappa \operatorname{Tr}(t_{DF}^2 \ln \frac{M_F}{\mu}), \quad (2.12)$$

and $\alpha_i = g_i^2/4\pi$. Here, $t_{D\psi}$ denotes the generators in the superheavy representation of \mathcal{G}_D with $\psi \in \{V, S, F\}$ referring to the vector, scalar, and fermion fields respectively with masses M_ψ . The above matching condition is modified if the daughter symmetry is an Abelian $U(1)_D$ and originates from multiple non-Abelian parent symmetries \mathcal{G}_{P_i} :

$$\frac{1}{\alpha_D(\mu)} = \sum_i \omega_i^2 \left(\frac{1}{\alpha_{P_i}(\mu)} - \frac{C_2(\mathcal{G}_{P_i})}{12\pi} \right) - \frac{\Lambda_D(\mu)}{12\pi}, \quad (2.13)$$

where the ω_i 's are the weight factors of the Abelian mixing with $\sum_i \omega_i^2 = 1$.

3 Symmetry Breaking and Topological Defects

In this paper we study two non-supersymmetric unified theories based on each of the gauge groups $SO(10)$ and E_6 with specific symmetry breaking chains. Regarding to notation, we denote a gauge group of the form $SU(m)_A \otimes SU(n)_B \otimes U(1)_C$ as $\mathcal{G}_{m_A n_B 1_C}$. Any representation under this product group is expressed as (p, q, r) , which implies that it transforms as p - and q -dimensional representation under $SU(m)_A$ and $SU(n)_B$ respectively carrying $U(1)_C$ charge r . For example, $\mathcal{G}_{2_L 2_R 4_C}$ stands for $SU(2)_L \otimes SU(2)_R \otimes SU(4)_C$ and the representation depicted as $(1, 3, 15)$ transforms as a singlet under $SU(2)_L$, a triplet under $SU(2)_R$, and as the adjoint representation under $SU(4)_C$. We will employ, throughout the paper, the so-called extended survival hypothesis which states that, at each stage of symmetry breaking, the only Higgs fields which do not decouple are the ones required for the subsequent symmetry breakings.

$SO(10)$ Unification through Two Intermediate Steps

The two symmetry breaking chains of $SO(10)$ considered in this paper are summarized in Fig. 1 together with the VEVs causing the breakings and the Higgs representations contributing to the RGEs at each stage. We first discuss the scenario where the $SO(10)$ is broken to $\mathcal{G}_{2_L 2_R 4_C}$ using the 210-plet VEV along its $(1, 1, 1)$ component, which also breaks D -parity [47] that interchanges the representations of $SU(2)_L$ and $SU(2)_R$ and conjugates that of $SU(4)_C$. So the unbroken group is denoted as $\mathcal{G}_{2_L 2_R 4_C \not{D}}$. To break $SU(4)_C$ to $\mathcal{G}_{3_C 1_{B-L}}$ and $SU(2)_R$ to $U(1)_R$, we employ the component $(1, 3, 15) \subset 210$, which produces $SU(4)_C$ and $SU(2)_R$ monopoles [7]. The breaking of $U(1)_{B-L} \otimes U(1)_R$ to $U(1)_Y$ is achieved by a VEV either along the component $(1, -\frac{1}{2}, 1, 1) \subset (1, 2, \bar{4})$ from a 16-plet of $SO(10)$, or the component $(1, 1, 1, -2) \subset (1, 3, 10)$ from a $\overline{126}$ -plet. These are two physically distinct cases [7]. In the former case, the $SU(4)_C$ and $SU(2)_R$ monopoles, if not inflated away, eventually come together to form a double charged monopole and no cosmic strings are produced. In the latter case, however, in addition to the

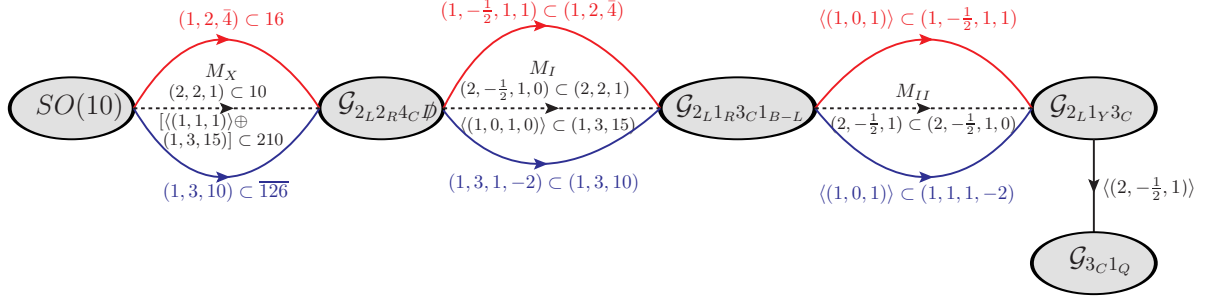


Figure 1: $SO(10)$ breaking to the SM via two intermediate steps. The VEVs causing the successive symmetry breakings and the Higgs fields contributing to the RGEs at each stage are indicated. The upper (red) arrows correspond to the model in Sec. 3.1, and the lower (blue) arrows correspond to the model in Sec. 3.2. The dashed arrows in the middle are common to both models.

monopoles, we have necklaces with $SU(4)_C$ and $SU(2)_R$ monopoles and antimonopoles as well as stable \mathbb{Z}_2 cosmic strings. For a recent study with a single intermediate step unification with Abelian mixing see Refs. [39, 41, 48].

In each of these cases the Abelian gauge coupling mixing is accounted for, as discussed in the previous section, by introducing a 2×2 gauge coupling matrix in the $(R, B-L \equiv X)$ space:

$$G = \begin{pmatrix} g_{RR} & g_{RX} \\ g_{XR} & g_{XX} \end{pmatrix}. \quad (3.1)$$

At the breaking scales M_I and M_{II} , the inverse squared gauge couplings $\omega(GG^T)^{-1}\omega^T$ are suitably projected to match with the parent or daughter inverse squared gauge couplings respectively. At M_I , we use the projectors $\omega = (1, 0)$ and $\omega = (0, 1)$ to match the inverse squared gauge couplings with $1/g_{2R}^2$ and $1/g_{4C}^2$ respectively, and, at M_{II} , we take $\omega = (\sqrt{3/5}, \sqrt{2/5})$ so that the inverse squared gauge couplings are projected on the hypercharge inverse squared gauge coupling. We consider the off-diagonal couplings

$$g_{RX} = g_{XR} = g \quad \text{and} \quad g_{XX}/g_{RR} = r \quad (3.2)$$

as free parameters in our subsequent analysis. Let us now discuss the two different breaking patterns of $SO(10)$ in turn.

3.1 $SO(10)$ without Strings or Necklaces

In the $SO(10)$ case with no strings or necklaces, the breaking of $SO(10)$ to $\mathcal{G}_{2_L 2_R 4_C D}$ is achieved by the VEV of the component $(1, 1, 1) \subset 210$. At this level, the component $(1, 3, 15) \subset 210$ remains massless. Also, the components $(2, 2, 1) \subset 10$ and $(1, 2, \bar{4}) \subset 16$. The next breaking to $\mathcal{G}_{2_L 1_R 3_C 1_{B-L}}$ is induced by the VEV of $(1, 3, 15) \subset 210$, and we are left with a single massless

electroweak Higgs doublet and a massless complex singlet $(1, -1/2, 1, +1) \subset (1, 2, \bar{4})$, whose VEV causes the subsequent breaking to the SM gauge symmetry. The $SO(10)$ breaking chain considered here can be depicted as follows:

$$SO(10) \xrightarrow[\langle 210 \rangle]{M_X} \mathcal{G}_{2_L 2_R 4_C \not{D}} \xrightarrow[\langle (1,3,15) \rangle \subset 210]{M_I} \mathcal{G}_{2_L 1_R 3_C 1_{B-L}} \xrightarrow[\langle (1, -\frac{1}{2}, 1, 1) \rangle \subset (1, 2, \bar{4}) \subset 16]{M_{II}} \mathcal{G}_{2_L 1_Y 3_C}.$$

The Higgs fields which remain massless at each stage of the symmetry breaking and thus contribute to the RGEs are summarized in Table 1. The β -coefficients and the RGEs are given in [Appendix](#).

$SO(10)$	$\mathcal{G}_{2_L 2_R 4_C \not{D}}$	$\mathcal{G}_{2_L 1_R 3_C 1_{B-L}}$	$\mathcal{G}_{2_L 1_Y 3_C}$
10	$(2, 2, 1)$	$(2, -\frac{1}{2}, 1, 0)$	$(2, -\frac{1}{2}, 1)$
16	$(1, 2, \bar{4})$	$(1, -\frac{1}{2}, 1, 1)$	
210	$(1, 3, 15)$		

Table 1: Higgs representations that contribute to the RGEs at each stage of the symmetry breaking for the $SO(10)$ model in Sec. 3.1.

3.2 $SO(10)$ with Strings and Necklaces

In the $SO(10)$ case with strings and necklaces, the breaking to $\mathcal{G}_{2_L 2_R 4_C \not{D}}$ is again achieved by the VEV of a scalar 210-plet. At this level we again have the massless components $(1, 3, 15) \subset 210$ and $(2, 2, 1) \subset 10$, but now a massless $(1, 3, 10) \subset 126$ too. The next breaking to $\mathcal{G}_{2_L 1_R 3_C 1_{B-L}}$ is induced by $(1, 3, 15)$, and we are left with a massless $(1, 1, 1, -2) \subset (1, 3, 10)$ and a single electroweak Higgs doublet. The VEV of $(1, 1, 1, -2)$ does the breaking to the SM gauge group. The $SO(10)$ breaking chain considered here can be depicted as follows:

$$SO(10) \xrightarrow[\langle 210 \rangle]{M_X} \mathcal{G}_{2_L 2_R 4_C \not{D}} \xrightarrow[\langle (1,3,15) \rangle \subset 210]{M_I} \mathcal{G}_{2_L 1_R 3_C 1_{B-L}} \xrightarrow[\langle (1,1,1,-2) \rangle \subset (1,3,10) \subset \bar{126}]{M_{II}} \mathcal{G}_{2_L 1_Y 3_C}.$$

The Higgs fields which contribute to the RGEs are summarized in Table 2. The β -coefficients and the RGEs are given in [Appendix](#).

$SO(10)$	$\mathcal{G}_{2_L 2_R 4_C \not{D}}$	$\mathcal{G}_{2_L 1_R 3_C 1_{B-L}}$	$\mathcal{G}_{2_L 1_Y 3_C}$
10	$(2, 2, 1)$	$(2, -\frac{1}{2}, 1, 0)$	$(2, -\frac{1}{2}, 1)$
$\bar{126}$	$(1, 3, 10)$	$(1, 1, 1, -2)$	
210	$(1, 3, 15)$		

Table 2: Higgs representations that contribute to the RGEs at each stage of the symmetry breaking for the $SO(10)$ model in Sec. 3.2.

E_6 Unification with Two Intermediate Steps

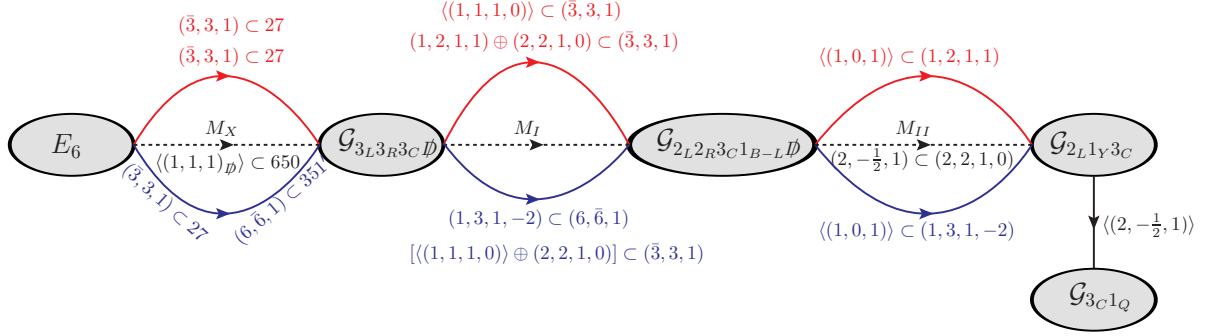


Figure 2: E_6 breaking to the SM with two intermediate steps. The VEVs and the Higgs fields contributing to the RGEs at each stage are indicated. The upper (red) arrows correspond to the model in Sec. 3.3, and the lower (blue) arrows correspond to the model in Sec. 3.4. The dashed arrows in the middle are common to both models.

The two symmetry breaking patterns of E_6 discussed here are summarized in Fig. 2 together with the VEVs causing the various symmetry breakings and the Higgs representations contributing to the RGEs at each stage. The E_6 gauge symmetry is broken to \mathcal{G}_{3L3R3C} using the D -violating VEV of a Higgs 650-plet. The next breaking to $\mathcal{G}_{2L2R3C1B-L}$ is achieved using a $(\bar{3}, 3, 1) \subset 27$ which, interestingly, is the $SO(10)$ singlet within the 27-plet of E_6 . The breaking to the SM gauge group though is induced through the VEV of a suitable sub-multiplet of a 27 or alternatively of a $351'$. From the perspective of emergence of possible topological defects, these are two distinct cases [7]. In the former case, i.e. with the Higgs 27-plet, we have single and triply charged monopoles. But in the latter case, i.e. with a scalar $351'$, we also have \mathbb{Z}_2 strings but not necklaces. We now discuss these two cases of E_6 breaking in turn.

3.3 E_6 without Strings

Let us first consider the E_6 case without strings. We use a Higgs 650-plet to break E_6 to \mathcal{G}_{3L3R3C} . At this level, we are left with two massless Higgs $(\bar{3}, 3, 1)$ from the two 27-plets. The breaking of \mathcal{G}_{3L3R3C} to $\mathcal{G}_{2L2R3C1B-L}$ is achieved through the VEV of the component $(1, 1, 1, 0)$ in $(\bar{3}, 3, 1)$. Noting the following decompositions of the $SU(3)_L$ and $SU(3)_R$ gauge bosons $(8, 1, 1) = (1, 1, 1, 0) \oplus (3, 1, 1, 0) \oplus (2, 1, 1, \pm 1)$, and $(1, 8, 1) = (1, 1, 1, 0) \oplus (1, 3, 1, 0) \oplus (1, 2, 1, \pm 1)$, it is evident that the nine would be Goldstone modes must transform as $(2, 1, 1, \pm 1)$, $(1, 2, 1, \pm 1)$, and one linear combination of two singlets. The components $(1, 2, 1, +1)$ and $(2, 2, 1, 0)$ belonging to the other $(\bar{3}, 3, 1)$ remain massless. The breaking of $\mathcal{G}_{2L2R3C1B-L}$ to the SM gauge group is achieved by employing the $(1, 2, 1, +1)$ component. One linear combination of the $SU(2)_L$ doublets in the bi-doublet $(2, 2, 1, 0)$ provides the electroweak Higgs doublet. The breaking

chain of E_6 considered here can be depicted as follows:

$$E_6 \xrightarrow[\langle 650 \rangle]{M_X} \mathcal{G}_{3_L 3_R 3_C} \xrightarrow[\langle (\bar{3}, 3, 1) \rangle \subset 27]{M_I} \mathcal{G}_{2_L 2_R 3_C 1_{B-L}} \xrightarrow[\langle (1, 2, 1, 1) \rangle \subset (\bar{3}, 3, 1) \subset 27]{M_{II}} \mathcal{G}_{2_L 1_Y 3_C}.$$

In Table 3, we summarize the Higgs representations that contribute to the RGEs at each stage.

E_6	$\mathcal{G}_{3_L 3_R 3_C}$	$\mathcal{G}_{2_L 2_R 3_C 1_{B-L}}$	$\mathcal{G}_{2_L 1_Y 3_C}$
27	$(\bar{3}, 3, 1)$	$(2, 2, 1, 0)$	$(2, -\frac{1}{2}, 1)$
27	$(\bar{3}, 3, 1)$	$(1, 2, 1, 1)$	
650			

Table 3: Higgs representations that contribute to the RGEs at each stage of the symmetry breaking for the E_6 model in Sec. 3.3.

The relevant β -coefficients are given as:

$$\text{From } M_{II} \text{ to } M_I : b_{2L} = -3, b_{2R} = -\frac{17}{6}, b_{3C} = -7, b_{B-L} = \frac{17}{4}, b_{ij} = \begin{pmatrix} 8 & 3 & 12 & \frac{3}{2} \\ 3 & \frac{61}{6} & 12 & \frac{9}{4} \\ \frac{9}{2} & \frac{9}{2} & -26 & \frac{1}{2} \\ \frac{9}{2} & \frac{27}{4} & 4 & \frac{37}{8} \end{pmatrix}.$$

$$\text{From } M_I \text{ to } M_X : b_{3L} = -4, b_{3R} = -4, b_{3C} = -5, b_{ij} = \begin{pmatrix} 34 & 28 & 12 \\ 28 & 34 & 12 \\ 12 & 12 & 12 \end{pmatrix}.$$

3.4 E_6 with Strings

In order to have cosmic strings, we break E_6 to $\mathcal{G}_{3_L 3_R 3_C}$ by again employing a scalar 650-plet, but at this level we are left with the following Higgs massless modes: $(\bar{3}, 3, 1) \subset 27$ and $(6, \bar{6}, 1) \subset 351'$. The breaking of $\mathcal{G}_{3_L 3_R 3_C}$ to $\mathcal{G}_{2_L 2_R 3_C 1_{B-L}}$ is again achieved by the VEV of $(1, 1, 1, 0) \subset (\bar{3}, 3, 1)$, and we are left with two massless Higgs representations, namely $(2, 2, 1, 0) \subset (\bar{3}, 3, 1)$ and $(1, 3, 1, -2) \subset (6, \bar{6}, 1)$. The latter component breaks $\mathcal{G}_{2_L 2_R 3_C 1_{B-L}}$ to the SM gauge group and we end up with a massless SM Higgs doublet from the former sub-multiplet, as in the previous cases. The breaking chain of E_6 considered here can be depicted as follows:

$$E_6 \xrightarrow[\langle 650 \rangle]{M_X} \mathcal{G}_{3_L 3_R 3_C} \xrightarrow[\langle (\bar{3}, 3, 1) \rangle \subset 27]{M_I} \mathcal{G}_{2_L 2_R 3_C 1_{B-L}} \xrightarrow[\langle (1, 3, 1, -2) \rangle \subset (6, \bar{6}, 1) \subset 351']{M_{II}} \mathcal{G}_{2_L 1_Y 3_C}.$$

The Higgs fields contributing to the RGEs at each stage are presented in Table 4

E_6	$\mathcal{G}_{3_L 3_R 3_C \cancel{D}}$	$\mathcal{G}_{2_L 2_R 3_C 1_{B-L} \cancel{D}}$	$\mathcal{G}_{2_L 1_Y 3_C}$
27	$(\bar{3}, 3, 1)$	$(2, 2, 1, 0)$	$(2, -\frac{1}{2}, 1)$
351'	$(6, \bar{6}, 1)$	$(1, 3, 1, -2)$	
650			

Table 4: Higgs representations that contribute to the RGEs at each stage of the symmetry breaking for the E_6 model in Sec. 3.4.

The necessary β -coefficients of the relevant RGEs are:

$$\text{From } M_{II} \text{ to } M_I : \quad b_{2L} = -3, \quad b_{2R} = -\frac{7}{3}, \quad b_{3C} = -7, \quad b_{B-L} = \frac{11}{2}, \quad b_{ij} = \begin{pmatrix} 8 & 3 & 12 & \frac{3}{2} \\ 3 & \frac{80}{3} & 12 & \frac{27}{2} \\ \frac{9}{2} & \frac{9}{2} & -26 & \frac{1}{2} \\ \frac{9}{2} & \frac{81}{2} & 4 & \frac{61}{2} \end{pmatrix}.$$

$$\text{From } M_I \text{ to } M_X : \quad b_{3L} = \frac{1}{2}, \quad b_{3R} = \frac{1}{2}, \quad b_{3C} = -5, \quad b_{ij} = \begin{pmatrix} 253 & 220 & 12 \\ 220 & 253 & 12 \\ 12 & 12 & 12 \end{pmatrix}.$$

4 Unification with Threshold Corrections and Proton Decay

We aim to find the unification solutions in terms of the unified gauge coupling constant g_U , the unification scale M_X , and the intermediate scales $M_{I,II}$ that are consistent with the experimental observables at the Z gauge boson mass m_Z . To perform this task, we define a χ^2 statistic at m_Z as

$$\chi^2 = \sum_{i=1}^3 \frac{(g_i^2 - g_{i,\text{exp}}^2)^2}{\sigma_{g_{i,\text{exp}}}^2}, \quad (4.1)$$

which we minimize to find the unification solutions. Here, g_i ($i = Y, 2L, 3C$) are the SM gauge couplings at m_Z and are related to the unification and intermediate scales and the unified gauge coupling through the RGEs. On the other hand, $g_{i,\text{exp}}^2$ are their experimental values squared computed from the electroweak observables along with the standard deviations denoted by σ – see Table 5. This method ensures that our unification solutions are consistent with the

Z -boson mass m_Z	91.1876(21) GeV
Strong fine structure constant α_{3C}	0.1185(6)
Fermi coupling constant G_F	$1.1663787(6) \times 10^{-5} \text{ GeV}^{-2}$
Weinberg angle $\sin^2 \theta_W$	0.23126(5)

Table 5: Experimental observables at m_Z .

electroweak observables [49]. We have taken the solutions for which the $\chi_{\min}^2 < 1$.

In the E_6 case, we add suitable threshold corrections while implementing the matching conditions at the breaking scales. Without loss of generality, we assume that the ratio of the mass of the heavy fields belonging to the parent symmetry to the symmetry breaking scale μ , i.e. M_i/μ ($i = V, S, F$ with notation as in Eq. (2.12)), varies within the range $[1/2, 2]$. In the case of the $SO(10)$ breaking chains, the presence of the Abelian mixing leads to a range of allowed solutions. Thus, additional contributions due to threshold corrections can be ignored to reduce the number of free parameters. In passing, we would like to mention that inclusion of threshold corrections will only widen the allowed parameter space without invalidating our conclusion.

One of the most interesting predictions of GUTs is the possibility of proton decay, which is unfortunately yet to be observed. In the ongoing experiments, the proton lifetime is continuously pushed to larger values that, in turn, puts severe constraints on the unification scale. Our aim is to find the unification solutions that are simultaneously compatible with the low energy observables and the exclusion limits on proton lifetime. Here, we consider the decay of proton into a positron and a neutral pion. The partial lifetime for this channel is given as [50–56]

$$\tau_p = \left[\frac{m_p}{32\pi} \left(1 - \frac{m_{\pi^0}^2}{m_p^2} \right)^2 A_L^2 \frac{g_U^4}{4M_X^4} (1 + |V_{ud}|^2)^2 \times \left(A_{SR}^2 |\langle \pi^0 | (ud)_{RuL} | p \rangle|^2 + A_{SL}^2 |\langle \pi^0 | (ud)_{LuL} | p \rangle|^2 \right) \right]^{-1}, \quad (4.2)$$

where g_U is the unified gauge coupling, and m_p and m_{π^0} are the masses of the proton and neutral pion respectively. The coefficients $A_{SR(SL)}$ include the enhancement factors due to the RGEs for proton decay operators from M_X to m_Z [53, 57–62], and A_L denotes the renormalization factor from m_Z to the QCD scale (~ 1 GeV) [63]. The Cabibbo–Kobayashi–Maskawa matrix element V_{ud} is given by $|V_{ud}| = 0.9742$ [49] and the form factors are taken from the lattice QCD computation of Ref. [64]:

$$\langle \pi^0 | (ud)_{RuL} | p \rangle = -0.131, \quad \langle \pi^0 | (ud)_{LuL} | p \rangle = 0.134. \quad (4.3)$$

We construct the unification solutions with unification scale up to $M_X = 10^{17}$ GeV which are consistent with all the constraints mentioned above for each of the symmetry breaking chains in Secs. 3.1, 3.2, 3.3, and 3.4 and depict them in Figs. 3, 4, 5, and 6 respectively. In particular, we present the allowed values of the unification scale M_X and the partial proton lifetime τ_p as functions of M_I and M_{II} . We note that the unified gauge coupling g_U lies within the range $[0.52, 0.53]$ for the two $SO(10)$ breaking chains in Secs. 3.1 and 3.2. In the case of E_6 , g_U ranges within $[0.51, 0.54]$ and $[0.51, 0.56]$ for the models in Secs. 3.3 and 3.4 respectively. In $SO(10)$, where we have Abelian mixing at the second intermediate symmetry breaking, we find unification solutions for g within $[0.40, 0.60]$ and $[0.39, 0.59]$ for the models in Secs. 3.1 and 3.2 respectively, and $r \in [0, 1]$ for both cases – for the definition of g and r

see Eq. (3.2). For the breaking chain in Sec. 3.1, we find that the intermediate scales lie in the ranges $\log_{10}(M_I/\text{GeV}) \in [16.1, 16.8]$ and $\log_{10}(M_{II}/\text{GeV}) \in [4.0, 16.0]$, and for the chain in Sec. 3.2 in the ranges $\log_{10}(M_I/\text{GeV}) \in [16.1, 16.7]$ and $\log_{10}(M_{II}/\text{GeV}) \in [4.0, 16.0]$. For E_6 , we obtain the intermediate scales for the model in Sec. 3.3 in the ranges $\log_{10}(M_I/\text{GeV}) \in [14.3, 16.9]$ and $\log_{10}(M_{II}/\text{GeV}) \in [9.4, 13.4]$, and for the chain in Sec. 3.4 in the ranges $\log_{10}(M_I/\text{GeV}) \in [11.6, 17.0]$ and $\log_{10}(M_{II}/\text{GeV}) \in [5.6, 14.6]$. At this point, we have verified that all the unification solutions satisfy the present Super-Kamiokande limit ($\tau_p > 1.6 \times 10^{34}$ years) [65, 66], and also the projected Hyper-Kamiokande limit ($\tau_p > 8.0 \times 10^{34}$ years) [67]. In the next section, we will find the ranges of M_X , M_I , and M_{II} for which a successful GUT-inflation scenario with a Coleman-Weinberg potential is compatible with the Planck satellite results [68].

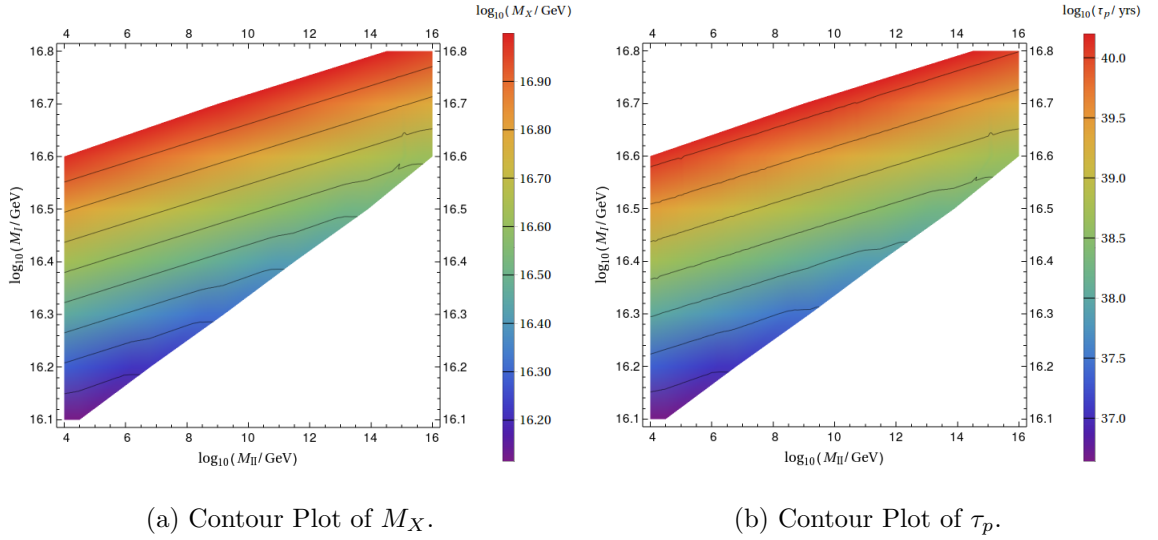


Figure 3: Contour plots for the $SO(10)$ breaking chain in Sec. 3.1, where the symmetry breaking $\mathcal{G}_{2_L 1_R 3_C 1_{B-L}} \rightarrow \mathcal{G}_{2_L 1_Y 3_C}$ at M_{II} is achieved by the VEV of $(1, -1/2, 1, 1) \subset 16$. For this fit, we have $g_U \in [0.52, 0.53]$, $r \in [0, 1]$, and $g \in [0.40, 0.60]$.

5 Inflation with Coleman-Weinberg Potential

In order to understand the inflationary dynamics, we consider the relevant part of the scalar potential [25, 26, 69]

$$V = \frac{\lambda}{4}\phi^4 - \frac{1}{2}\beta^2\phi^2\chi^2 + \frac{a}{4}\chi^4 + A\phi^4 \left[\log\left(\frac{\phi}{M}\right) + c \right] + V_0, \quad (5.1)$$

where the GUT-singlet inflaton field ϕ and the GUT symmetry breaking scalar χ are canonically normalized real scalar fields, and $A = \beta^4 D/16\pi^2$ [7], with D being the dimensionality of the

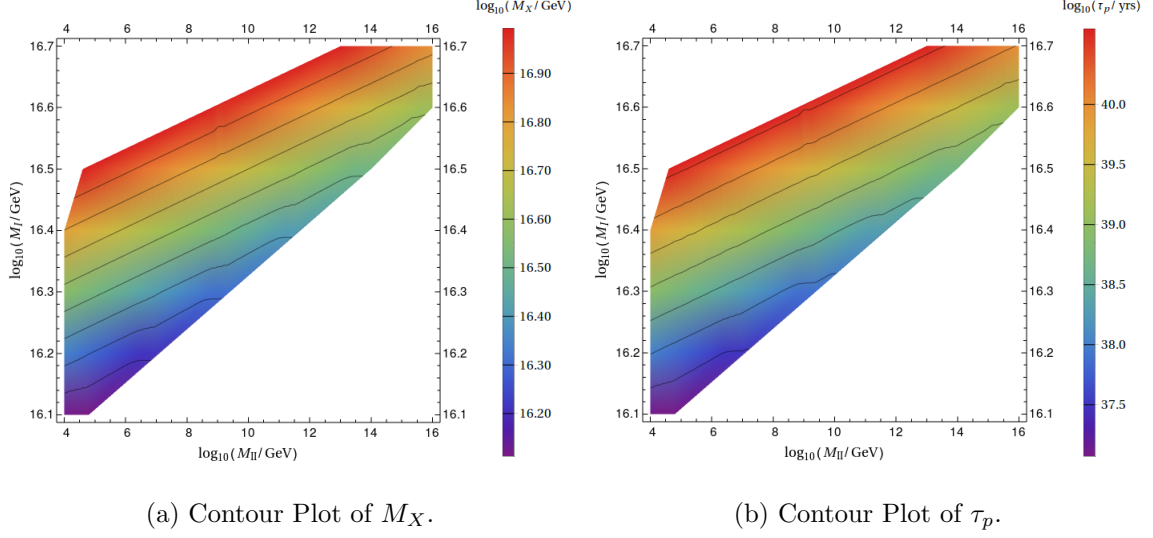


Figure 4: Contour plots for the $SO(10)$ breaking chain in Sec. 3.2, where the VEV of $(1, 1, 1, -2) \subset \overline{126}$ breaks $\mathcal{G}_{2_L 1_R 3_C 1_{B-L}}$ to $\mathcal{G}_{2_L 1_Y 3_C}$. For this fit, we have $g_U \in [0.52, 0.53]$, $r \in [0, 1]$, and $g \in [0.39, 0.59]$.

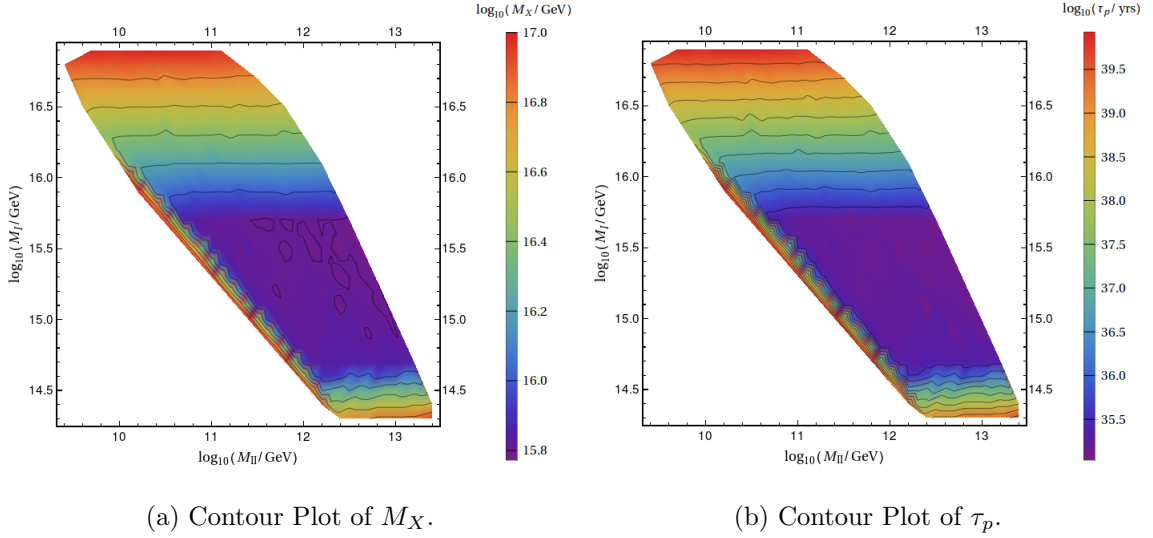


Figure 5: Contour plots for the E_6 breaking chain in Sec. 3.3, where the VEV of $(1, 2, 1, 1) \subset 27$ causes the symmetry breaking $\mathcal{G}_{2_L 2_R 3_C 1_{B-L}} \rightarrow \mathcal{G}_{2_L 1_Y 3_C}$ at M_{II} . For this fit, $g_U \in [0.51, 0.54]$.

representation to which χ belongs. We substitute $\chi = (\beta/\sqrt{a})\phi$ in Eq. (5.1), which minimizes the potential for any given value of ϕ . In the limit $\lambda \ll \beta^4$ and requiring that the potential is

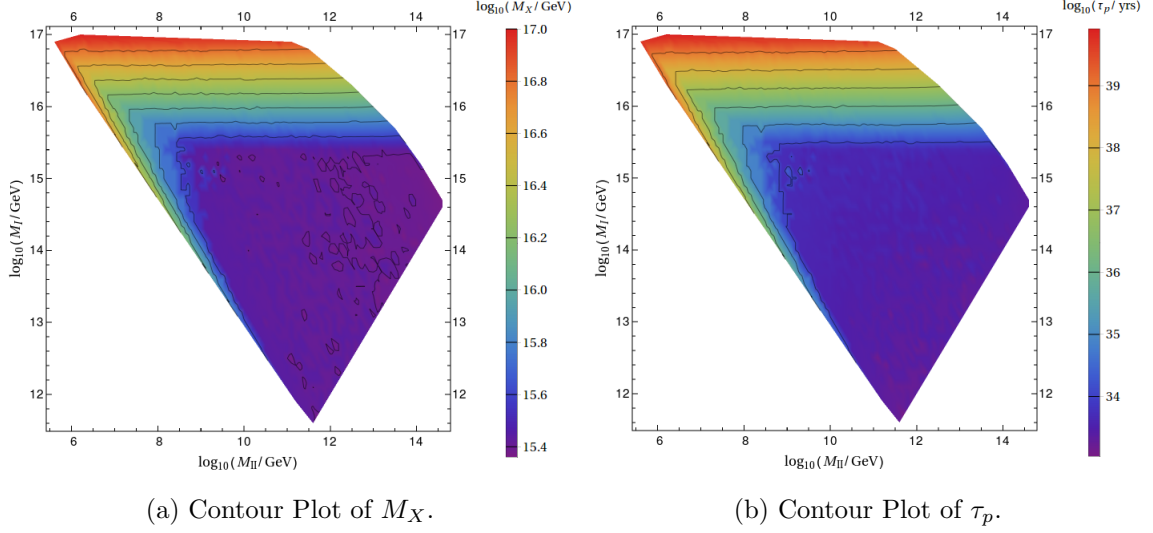


Figure 6: Contour plots for the E_6 breaking chain in Sec. 3.4, where the VEV of $(1, 3, 1, -2) \subset 351'$ causes the symmetry breaking $\mathcal{G}_{2_L 2_R 3_C 1_{B-L}} \rightarrow \mathcal{G}_{2_L 1_Y 3_C}$ at M_{II} . For this fit, $g_U \in [0.51, 0.56]$.

minimized at $\phi = M$ with $V(\phi = M) = 0$, we find

$$V(\phi) = A\phi^4 \left[\log\left(\frac{\phi}{M}\right) - \frac{1}{4} \right] + \frac{AM^4}{4}, \quad (5.2)$$

where $V_0 = AM^4/4$.

The slow-roll parameters can be written in terms of the potential and its derivatives as follows (for a review see Ref. [70]):

$$\epsilon = \frac{m_{\text{Pl}}^2}{2} \left(\frac{V'}{V} \right)^2, \quad \eta = m_{\text{Pl}}^2 \frac{V''}{V}, \quad \xi^2 = m_{\text{Pl}}^4 \frac{V'V'''}{V^2}, \quad (5.3)$$

where m_{Pl} is the reduced Planck scale and primes represent derivatives with respect to ϕ . The spectral index n_s , the tensor-to-scalar ratio r , and the running of the spectral index $\alpha \equiv dn_s/d \ln k$ can be deduced using the slow-roll parameters computed at the pivot scale k_* :

$$n_s = 1 - 6\epsilon_* + 2\eta_*, \quad r = 16\epsilon_*, \quad \alpha = 16\epsilon_*\eta_* - 24\epsilon_*^2 - 2\xi_*^2. \quad (5.4)$$

Here, the subscript $*$ signifies the values of the parameters at the pivot scale $k_* = 0.05 \text{ Mpc}^{-1}$. The experimental values of these observables at 95% confidence level are as follows [68]:

$$n_s = 0.9658 \pm 0.0080, \quad r < 0.068, \quad \text{and} \quad \alpha = -0.0066 \pm 0.0140. \quad (5.5)$$

The amplitude of the curvature perturbation Δ_R is given by

$$\Delta_R^2 = \frac{1}{12\pi^2 m_{\text{Pl}}^6} \left. \frac{V^3}{(V')^2} \right|_{\phi=\phi_*}, \quad (5.6)$$

with its experimental value $\Delta_R^{2\text{exp}} = (2.099 \pm 0.101) \times 10^{-9}$ at 95% confidence level [68].

The number of e -foldings for the pivot scale is computed using the following equation:

$$N_* = \frac{1}{m_{\text{Pl}}^2} \int_{\phi_e}^{\phi_*} \frac{V d\phi}{V'}. \quad (5.7)$$

Here ϕ_e is the value of ϕ at the end of inflation and is deduced using the following condition:

$$\max(|\eta|, \epsilon) = 1. \quad (5.8)$$

The number of e -foldings for the pivot scale $k_* = 0.05 \text{ Mpc}^{-1}$ can alternatively be obtained from the knowledge of the thermal history of the universe [71]:

$$N_* \simeq 61.5 + \frac{1}{2} \ln \frac{\rho_*}{m_{\text{Pl}}^4} - \frac{1}{3(1+\omega_r)} \ln \frac{\rho_e}{m_{\text{Pl}}^4} + \left(\frac{1}{3(1+\omega_r)} - \frac{1}{4} \right) \ln \frac{\rho_r}{m_{\text{Pl}}^4}, \quad (5.9)$$

where $\rho_* = V(\phi_*)$, $\rho_e = V(\phi_e)$, and $\rho_r = (\pi^2/30)g_*T_r^4$ are the energy densities at the pivot scale, at the end of inflation, and at the reheat temperature T_r , respectively, and ω_r is the effective equation-of-state parameter from the end of inflation until reheating. The effective number of massless degrees of freedom g_* at reheating is taken to be 106.75 corresponding to the SM spectrum. Clearly, the values of N_* from Eqs. (5.7) and (5.9) must coincide. For our analysis, we consider the so-called middle- N scenario (see Ref. [72]), where $T_r = 10^9 \text{ GeV}$ and $\omega_r = 0$.

In order to find consistent inflationary solutions in terms of the parameters A , M , ϕ_* , and ϕ_e , we construct a χ^2 function and adopt the following steps:

(i) We write

$$A = 4V_0/M^4, \quad M_X = \sqrt{8\pi/a}(V_0/D)^{1/4}, \quad (5.10)$$

and express ϵ as a function of M , and ϕ . The value ϕ_e of ϕ at the end of inflation is then determined by requiring that $\epsilon(M, \phi_e) = 1$.

(ii) We express n_s as a function of M , ϕ_* , and Δ_R^2 as a function of V_0 , M , ϕ_* .

(iii) We compute N_* as a function of M , ϕ_* , ϕ_e from Eq. (5.7) and as a function of V_0 , M , ϕ_* , ϕ_e using Eq. (5.9). We then require that both results coincide up to a numerical tolerance ΔN_* .

(iv) We choose the following values for the observables:

$$(a) \Delta_R^{2\text{exp}} \pm \delta(\Delta_R^{2\text{exp}}) = (2.099 \pm 0.101) \times 10^{-9},$$

$$\begin{aligned}
(b) \quad \epsilon(\phi_e) \pm \delta(\epsilon(\phi_e)) &= 1.0 \pm 0.1, \\
(c) \quad \Delta N_* \pm \delta(\Delta N_*) &= 0.0 \pm 1.0,
\end{aligned} \tag{5.11}$$

for given values of V_0 and the other parameters M , ϕ_* , and ϕ_e . We ensure that the arbitrary choice of tolerance for $\epsilon(\phi_e)$ and ΔN_* does not affect our conclusions.

(v) We define χ^2 as a function of M , ϕ_* , and ϕ_e for some benchmark choices of V_0 :

$$\chi^2 = \frac{(\Delta_R^2 - \Delta_R^{2\text{exp}})^2}{(\delta(\Delta_R^{2\text{exp}}))^2} + \frac{(\epsilon(\phi_e) - 1.0)^2}{(\delta\epsilon(\phi_e))^2} + \frac{(\Delta N_*)^2}{(\delta(\Delta N_*))^2}. \tag{5.12}$$

We minimize the χ^2 function to find the best fit values of M , ϕ_* , and ϕ_e for a specific choice of $V_0^{1/4}$. In the process of minimization, we also ensure that ϵ converges to unity before $|\eta|$ as ϕ approaches ϕ_e .

(vi) Finally, using the best-fit values of the parameters, we estimate A from Eq. (5.10) and, subsequently, reconstruct the potential using Eq. (5.2). We further compute the slow-roll parameters from Eq. (5.3) and also n_s , r , and α from Eq. (5.4).

$\frac{V_0^{1/4}}{10^{16}\text{GeV}}$	$\frac{V(\phi_*)^{1/4}}{10^{16}\text{GeV}}$	$\log_{10} A$	M/m_{Pl}	ϕ_*/m_{Pl}	ϕ_e/m_{Pl}	N_*	$\Delta_R^2 \times 10^9$	n_s	r	$\alpha \times 10^4$
1.51	1.44	-13.4	20.20	9.13	18.87	52.3	2.1	0.9584	0.039	-6.41
1.59	1.50	-13.5	21.89	10.52	20.55	52.3	2.1	0.9596	0.045	-6.40
1.66	1.55	-13.6	23.81	12.17	22.47	52.4	2.1	0.9606	0.052	-6.41
1.74	1.59	-13.6	26.01	14.09	24.65	52.4	2.1	0.9615	0.058	-6.44
1.82	1.64	-13.7	28.50	16.33	27.15	52.5	2.1	0.9623	0.065	-6.49

Table 6: Values of the parameters for successful inflation with a Coleman-Weinberg potential.

In Table 6, we present the estimated values of the various parameters of the model including the slow-roll parameters, which are within two standard deviations from their central experimental values – see Eqs. (5.5) and (5.11). The range of the corresponding V_0 is $V_0^{1/4}/10^{16} \text{ GeV} \in [1.51, 1.82]$. We see that these solutions are perfectly compatible with all the requirements for a successful inflation. At this point it is worth mentioning that the minimum values of χ^2 are found to be $\chi_{\min}^2 \sim 10^{-13} \ll 1$ for the fitted parameters in Table 6. Recall that the first step of symmetry breaking of $SO(10)$ and E_6 is achieved by the 210- and 650-dimensional representation, respectively. Therefore, using Eq. (5.10), we find that the unification scale M_X is given by $M_X = 2.342 V_0^{1/4}$ for $SO(10)$ and $M_X = 1.766 V_0^{1/4}$ for E_6 . Thus, the range of the unification scale for successful inflation is $\log_{10}(M_X/\text{GeV}) \in [16.55, 16.63]$ and $\log_{10}(M_X/\text{GeV}) \in [16.43, 16.51]$ for $SO(10)$ and E_6 , respectively, which are compatible with the present Super-Kamiokande [65] and future Hyper-Kamiokande [67] bounds on proton lifetime.

Before concluding this section let us emphasize that the tensor-to-scalar ratio r is predicted to lie somewhere around $0.03 - 0.06$ – see Table 6. In the presence of non-minimal coupling to gravity, r can approach values close to 0.003 [73, 74].

6 Phase Transitions and Formation of Topological Defects

The first step of the spontaneous breaking of E_6 and $SO(10)$ is achieved through the VEV of a suitable GUT non-singlet canonically normalized real scalar field χ , which sets the value of the unification scale $\langle\chi\rangle \equiv M_X = (\beta/\sqrt{a})M$. We chose χ to belong to a 650- or 210-plet of E_6 or $SO(10)$, respectively. At this point a legitimate question to ask is when the actual GUT phase transition takes place. In the absence of temperature corrections, the potential is minimized at $\langle\chi\rangle = \pm(\beta/\sqrt{a})\phi$ for any given value of ϕ . Thus, the field χ remains non-zero as ϕ rolls towards M from non-zero values. However, during inflation, we must include in the potential the temperature correction $(1/2)\sigma_\chi T_H^2 \chi^2$ [25], where $T_H = H/2\pi$ is the Hawking temperature and σ_χ is assumed to be of order unity. Initially, ϕ is small and this correction term dominates over the second term in the right hand side of Eq. (5.1). Consequently, the potential attains its minimum at $\chi = 0$ with the GUT gauge symmetry restored. But as ϕ grows, $\chi = 0$ turns into a local maximum of the potential and two global minima appear at

$$\chi = \pm\sqrt{[\beta^2\phi^2 - \sigma_\chi T_H^2]/a} . \quad (6.1)$$

The potential difference between the local maximum at $\chi = 0$ and these minima is

$$\Delta V = (\beta^2\phi^2 - \sigma_\chi T_H^2)^2/4a. \quad (6.2)$$

At the beginning, these minima are very shallow and the fluctuations between them over the local maximum are very frequent. The fluctuations occur within spheres of radii equal to the Higgs correlation length m_{eff}^{-1} , with m_{eff} being the effective mass of χ at the minima given by

$$m_{\text{eff}}^2 = 2[\beta^2\phi^2 - \sigma_\chi T_H^2]. \quad (6.3)$$

These fluctuations are Boltzmann suppressed when the energy required is higher than T_H . This gives the so-called Ginzburg criterion [75]:

$$\frac{4\pi}{3}m_{\text{eff}}^{-3}\Delta V > T_H \Rightarrow \beta^2\phi^2 > \left(\frac{72a^2}{\pi^2} + \sigma_\chi\right)T_H^2. \quad (6.4)$$

At the value of ϕ saturating this inequality, χ settles down in one of the vacua and the breaking of the GUT gauge symmetry is completed leading to the formation of topological defects.

The next (first intermediate) step of symmetry breaking is induced by the VEV of another canonically normalized real scalar field χ_I , which belongs to an appropriate representation of the intermediate gauge symmetry. For example, the field that breaks the $\mathcal{G}_{2_L 2_R 4_C}$ symmetry lies in $(1, 3, 15)$ contained in a 210-plet of $SO(10)$. Similar to the previous case, the potential for χ_I is

$$V(\phi, \chi_I) = -\frac{1}{2}\beta_I^2\phi^2\chi_I^2 + \frac{a_I}{4}\chi_I^4, \quad (6.5)$$

with the final VEV

$$\langle \chi_I \rangle \equiv M_I = \frac{\beta_I}{\sqrt{a_I}} M. \quad (6.6)$$

After incorporating the finite temperature correction $(1/2)\sigma_{\chi_I}T_H^2\chi_I^2$, the effective mass-squared of χ_I reads

$$m_{\text{eff}}^2 = 2[\beta^2\phi^2 - \sigma_{\chi_I}T_H^2]. \quad (6.7)$$

Therefore, the phase transition and the formation of the associated topological defects occur for

$$\beta_I^2\phi^2 = \left(\frac{72a_I^2}{\pi^2} + \sigma_{\chi_I} \right) T_H^2. \quad (6.8)$$

From this equation, we can estimate the first intermediate breaking scale M_I as:

$$M_I = \sqrt{\left(\frac{72a_I^2}{\pi^2} + \sigma_{\chi_I} \right)} \frac{H_I}{2\pi\phi_I} \frac{M}{\sqrt{a_I}}, \quad (6.9)$$

where ϕ_I is the value of the inflaton field at the phase transition, and H_I is the corresponding value of the Hubble parameter. We assume that $a_I^2 \sim 0.1$ and $\sigma_{\chi_I} \sim 1$.

Following similar steps, we display the potential for the scalar field χ_{II} whose VEV causes the second intermediate symmetry breaking:

$$V(\phi, \chi_{II}) = -\frac{1}{2}\beta_{II}^2\phi^2\chi_{II}^2 + \frac{a_{II}}{4}\chi_{II}^4. \quad (6.10)$$

The effective mass-squared for χ_{II} is

$$m_{\text{eff}}^{II^2} = 2[\beta^2\phi^2 - \sigma_{\chi_{II}}T_H^2], \quad (6.11)$$

and the second intermediate breaking scale is

$$M_{II} = \sqrt{\left(\frac{72a_{II}^2}{\pi^2} + \sigma_{\chi_{II}} \right)} \frac{H_{II}}{2\pi\phi_{II}} \frac{M}{\sqrt{a_{II}}}. \quad (6.12)$$

Here, the phase transition occurs for $\phi = \phi_{II}$ and H_{II} is the Hubble parameter at ϕ_{II} . We also choose $a_{II}^2 \sim 0.1$ and $\sigma_{\chi_{II}} \sim 1$.

At this point, it should be mentioned that the logarithmic terms in the Coleman-Weinberg potential arising from the couplings of ϕ to χ_I , χ_{II} can be ignored since $\beta_I, \beta_{II} \ll \beta$. Thus, we do not include them in our analysis.

7 Intermediate Mass Monopoles

All GUT models predict [7] the existence of topologically stable magnetic monopoles associated with the unification scale M_X . In addition, the $SO(10)$ model predicts the appearance of

intermediate mass monopoles carrying two quanta of Dirac magnetic charge associated with the first intermediate breaking scale M_I [7]. In the E_6 case, monopoles with a triple Dirac charge are generated at the first intermediate phase transition [7]. As we will see later, the GUT monopoles are entirely inflated away, and we will thus concentrate on the monopole production at the scale M_I and compare their predicted present abundance with the results of the MACRO experiment [76]. The upper bound on the monopole flux from this experiment is $2.8 \times 10^{-16} \text{ cm}^{-2} \text{ s}^{-1} \text{ sr}^{-1}$. We take the lower bound (or observability threshold) on the monopole flux to be $10^{-24} \text{ cm}^{-2} \text{ s}^{-1} \text{ sr}^{-1}$, below which the monopoles are too diluted to be observed. We define the monopole yield as $Y_M \equiv n_M/s$, where n_M and s are the monopole number density and the entropy density respectively. The MACRO bound on the monopole flux for monopole masses $m_M \sim 10^{14} \text{ GeV}$ then implies [77] that the maximum allowed Y_M is $Y_M^{\text{max}} \sim 10^{-27}$, while the observability threshold adopted here corresponds to the minimal value of the monopole yield $Y_M^{\text{min}} \sim 10^{-35}$.

We next turn to the discussion of monopole production at M_I and the subsequent evolution of their abundance [7, 69]. We assume that the mean inter-monopole distance at production is of order m_{eff}^{I-1} , such that the monopole number density is $\simeq (1/10)m_{\text{eff}}^{I3}$, where we included a numerical factor 1/10. The monopoles are subsequently diluted by the factors $\exp(-3N_I)$ and $(t_r/\tau)^2$ during inflation and inflaton oscillations respectively. Here, t_r is the reheate time, which is about 0.36 GeV^{-1} for $T_r = 10^9 \text{ GeV}$ and for the SM spectrum, and τ is the cosmic time at the end of inflation. The monopole number density at reheating is about $(m_{\text{eff}}^{I3}/10) \exp(-3N_I)(\tau/t_r)^2$, while the entropy density is $(2\pi^2/45)g_*T_r^3$. Using these estimates we can find the monopole yield $Y_M = n_M/s$ after reheating as a function of M_I :

$$Y_M \simeq \frac{\frac{m_{\text{eff}}^{I3}}{10} \exp(-3N_I) \left(\frac{\tau}{t_r}\right)^2}{\frac{2\pi^2}{45} g_* T_r^3} . \quad (7.1)$$

Here, $H_I^2 = V(\phi_I)/3m_{\text{Pl}}^2$, $N_I = (1/m_{\text{Pl}}^2) \int_{\phi_e}^{\phi_I} V d\phi/V'$, and $g_* = 106.75$ for the SM spectrum. Using the equation

$$3H\dot{\phi} + V'(\phi) \simeq 0 , \quad (7.2)$$

which holds during inflation to a good approximation, we can compute the time τ at the termination of inflation as follows:

$$\tau \simeq \int_{\phi_e}^{\phi_*} \frac{3H(\phi)}{V'} d\phi . \quad (7.3)$$

In Table 7, we present the minimal required numbers of e -foldings N_+ which must follow the monopole production so that the MACRO bound on the monopole flux is satisfied. We also show the corresponding lower bounds M_{I+} on M_I , as well as the corresponding values of the inflaton ϕ_+ , and the Hubble parameter H_+ at monopole production. We also estimate the values of these parameters (indicated by a subscript $-$) corresponding to the threshold for

$\frac{V_0^{1/4}}{10^{16}\text{GeV}}$	$\frac{\tau}{10^{-12}\text{GeV}^{-1}}$	ϕ_+/m_{Pl}	ϕ_-/m_{Pl}	$\frac{H_+}{(10^{13}\text{GeV})}$	$\frac{H_-}{(10^{13}\text{GeV})}$	N_+	N_-	$\log_{10}\left(\frac{M_{I+}}{\text{GeV}}\right)$	$\log_{10}\left(\frac{M_{I-}}{\text{GeV}}\right)$
1.51	1.38	14.41	13.07	3.40	3.91	9.8	16.2	13.30	13.40
1.59	1.32	16.04	14.67	3.54	4.10	9.9	16.2	13.30	13.41
1.66	1.26	17.91	16.51	3.67	4.28	9.9	16.2	13.31	13.41
1.74	1.22	20.05	18.62	3.78	4.45	9.9	16.2	13.31	13.41
1.82	1.18	22.51	21.04	3.88	4.59	9.9	16.2	13.31	13.41

Table 7: Values of the various parameters (indicated by a subscript +) corresponding to the MACRO bound on the flux of monopoles formed at the scale M_I and their values (indicated by a subscript −) corresponding to the adopted observability threshold for the monopole flux.

observability.

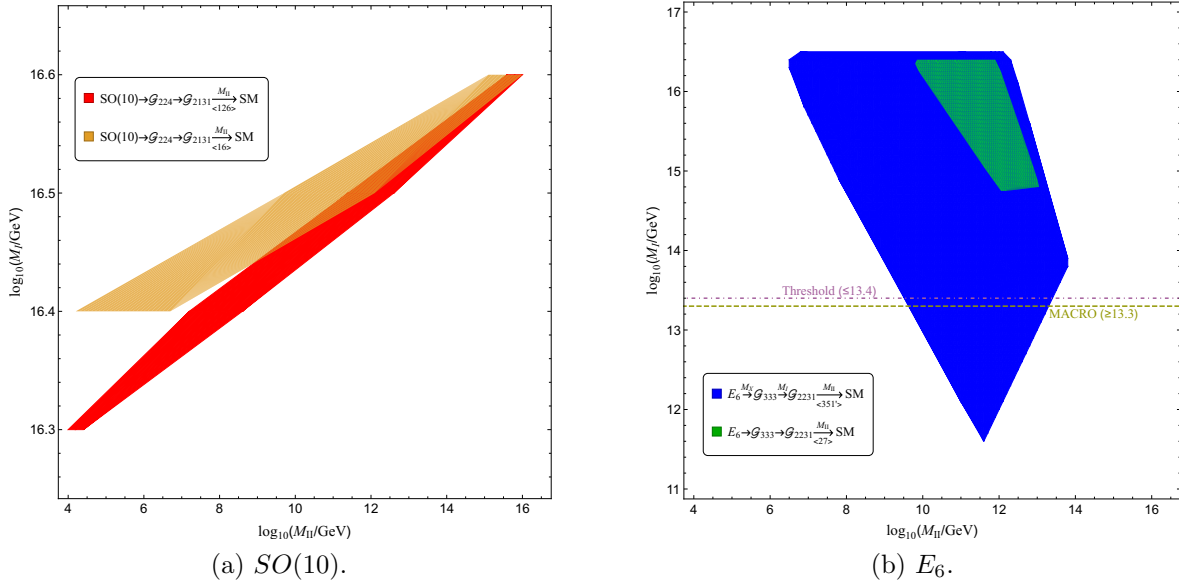


Figure 7: Intermediate breaking scales M_I and M_{II} for $\log_{10}(M_X/\text{GeV}) \in [16.55, 16.63]$ in the case of $SO(10)$ and $\log_{10}(M_X/\text{GeV}) \in [16.43, 16.51]$ in the case of E_6 with successful inflation based on a Coleman-Weinberg potential. We also show the two bounds M_{I+} and M_{I-} on M_I derived by using Eq. (6.9). Namely, the horizontal lines at $\log_{10}(M_{I+}/\text{GeV}) = 13.3$ (dashed) and $\log_{10}(M_{I-}/\text{GeV}) = 13.4$ (dot-dashed) represent the MACRO bound and the upper bound on M_I for observability of the monopole flux (for M_I 's above this value, the monopoles are too diluted to be observed).

In Fig. 7, we show the allowed ranges of the intermediate scales M_I , M_{II} which are consistent with successful inflation based on a Coleman-Weinberg potential for the four GUT scenarios considered with the unification scale M_X restricted in the range $\log_{10}(M_X/\text{GeV}) \in [16.55, 16.63]$ for $SO(10)$, and $\log_{10}(M_X/\text{GeV}) \in [16.43, 16.51]$ for E_6 . It should be mentioned that the unification scale is perfectly consistent with the proton lifetime bounds suggested by the present

Super-Kamiokande results as well as the expected sensitivity of the future Hyper-Kamiokande experiment. We note that out of the four scenarios only the E_6 unified model with \mathbb{Z}_2 strings can yield an observable flux of triply charged monopoles produced at the intermediate scale M_I . The MACRO bound excludes a considerable part of the available (blue) region for this model – see Fig. 7. It also suggests that the monopoles corresponding to the unification scale M_X are inflated away in all cases.

8 Intermediate Scale Strings and Gravity Waves

The \mathbb{Z}_2 cosmic strings are formed [7] at M_{II} when the parent symmetry is broken through the VEV of a sub-multiplet of $351'$ or $\overline{126}$ in E_6 or $SO(10)$ respectively. The mean inter-string distance d_s , i.e. the scale of the network, at formation is expected to be

$$d_s \simeq p m_{\text{eff}}^{II-1}, \quad (8.1)$$

where $p \simeq 2$ is a geometric factor. For generic values of M_{II} , these strings will be formed during inflation. But, for suitably lower M_{II} values, the strings can appear after the end of inflation, either during the inflaton oscillations or even after reheating.

We first investigate the situation with M_{II} large enough so that the string formation takes place during the inflationary era. From Eq. (6.12), we can find the lower bound on M_{II} for this to happen:

$$M_{II} > \sqrt{\left(\frac{72\alpha_{II}^2}{\pi^2} + \sigma_{\chi_{II}}\right)} \frac{H(\phi_e)}{2\pi} \frac{M}{\phi_e \sqrt{\alpha_{II}}}, \quad (8.2)$$

with $H(\phi_e) = \sqrt{V(\phi_e)/3m_{\text{Pl}}^2}$. The inflaton value $\phi = \phi_{II}$ at the phase transition can be computed again from Eq. (6.11). We then determine the effective scalar mass using Eq. (6.11) and the mean inter-string distance from Eq. (8.1). During inflation, d_s is scaled by a factor $\exp(N_{II})$, where $N_{II} = (1/m_{\text{Pl}}^2) \int_{\phi_e}^{\phi_{II}} V d\phi/V'$ is the number of e -foldings after the string formation. The inter-string distance gets further scaled by two additional factors, namely by $(t_r/\tau)^{2/3}$ during the period of inflaton oscillations and by T_r/T_0 from reheating to the present time, where $T_0 = 2.35 \times 10^{-13}$ GeV is the present cosmic microwave background temperature. Including these factors, we estimate the present value of d_s

$$d_s \simeq p m_{\text{eff}}^{II-1}(\phi_{II}) \exp(N_{II}) \left(\frac{t_r}{\tau}\right)^{\frac{2}{3}} \frac{T_r}{T_0}. \quad (8.3)$$

For strings to enter the present horizon, i.e. not to be inflated away, the inter-string distance in Eq. (8.3) should be smaller than the present horizon size $3t_0$, where $t_0 = 6.62 \times 10^{41}$ GeV $^{-1}$ is the present cosmic time.

The dimensionless string tension $G\mu$ is given by

$$G\mu \simeq \frac{1}{8} \left(\frac{M_{II}}{m_{\text{Pl}}} \right)^2, \quad (8.4)$$

where G and μ are Newton's constant and the string tension, i.e. the string mass per unit length, respectively. Here, our assumption is that these strings are close to the Bogomol'nyi limit of the Abelian Higgs model [78–80]. From PTA [17], we know that $G\mu \lesssim 1.5 \times 10^{-11}$ [18], which implies that $M_{II} \lesssim 2.7 \times 10^{13}$ GeV. (For recent developments see Refs. [21–24].) As we will see later, this bound is strictly applicable only to those strings that enter the horizon before $t \simeq 10\Gamma G\mu t_{eq}$ (Γ is a numerical factor of order 50), and certainly not for strings entering the horizon after the equidensity time $t_{eq} \simeq 2.253 \times 10^{36}$ GeV⁻¹, where the energy densities of radiation and matter coincide.

The mean inter-string distance at a cosmic temperature T after reheating and before the equidensity point can be estimated from Eq. (8.3) with T_0 replaced by T , where

$$T^2 = \sqrt{\frac{45}{2\pi^2}} g_*^{-1/2} \frac{m_{\text{Pl}}}{t}, \quad (8.5)$$

with the appropriate value of g_* for the relevant temperature range. Equating this inter-string distance with the horizon distance $2t$, we can calculate the scale M_{II} for which the strings enter the horizon at any given cosmic time t during radiation dominance. After horizon entrance the long strings chop each other and inter-commute generating loops of typical size $\ell \simeq t/10$ at any subsequent time t [81, 82]. These loops eventually decay [83] into gravity waves at $t \simeq \ell/\Gamma G\mu$, providing the major contribution to the stochastic background. Strings that enter the horizon before $10\Gamma G\mu t_{eq}$ give rise to a complete spectrum of loops generated between this time and t_{eq} and decaying after t_{eq} . These loops which are created during radiation dominance and decay during matter dominance generate [84] the overall peak of the stochastic gravity waves which lies at low frequencies and is restricted by the PTA bound.

In order to compute the scale M_{II} corresponding to strings entering the horizon after t_{eq} , we need to solve the inequality

$$3t_{eq} < p m_{eff}^{-1} \exp(N_{II}) \left(\frac{t_r}{\tau} \right)^{\frac{2}{3}} \left(\frac{T_r}{T_{eq}} \right), \quad (8.6)$$

where $T_{eq} = 9.45 \times 10^{-10}$ GeV is the temperature at t_{eq} . These strings may generate [84] an insignificant low frequency peak in the gravity wave spectrum which is overshadowed by the overall peak and thus they are not important for the PTA bound.

In Fig. 8, we show the values of the second intermediate scale M_{II} which correspond to strings generated during inflation that re-entered the horizon during different eras of the universe, consistent with successful inflation (see Table 6).

Let us summarize the various regions in Fig. 8:

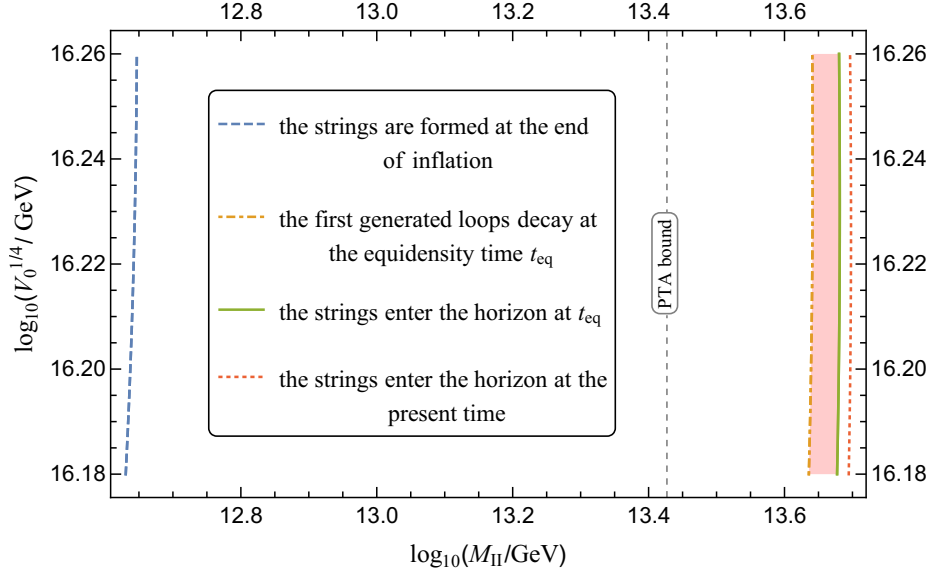


Figure 8: Intermediate breaking scales M_{II} for the unification scale $\log_{10}(V_0^{1/4}/\text{GeV}) \in [16.18, 16.26]$ for successful inflation with Coleman-Weinberg potential for different cases: 1. strings are formed at the end of inflation, 2. earliest loops decay at the equidensity time t_{eq} , 3. strings enter the horizon at t_{eq} , and 4. strings enter the horizon at the present time. The dashed black line corresponding to the PTA bound is also shown.

- For $\log_{10}(M_{II}/\text{GeV}) \gtrsim 12.64$, the phase transition takes place and strings are generated before the end of inflation.
- For $\log_{10}(M_{II}/\text{GeV}) \lesssim 13.64$, the strings enter the horizon before $t \simeq 10\Gamma G\mu t_{eq}$, and thus the loops generated after this time and before t_{eq} are present. These loops generate [84] a significant low frequency peak in the spectrum of stochastic gravity waves and the restriction from the PTA bound is expected to hold in this case. Loops created before $t \simeq 10\Gamma G\mu t_{eq}$ decay during radiation dominance and contribute [84] to the plateau of the spectrum.
- For $13.64 \lesssim \log_{10}(M_{II}/\text{GeV}) \lesssim 13.68$, the strings enter the horizon after $t \simeq 10\Gamma G\mu t_{eq}$ and before t_{eq} . Only part of the loops that are generated during radiation dominance and decay after t_{eq} are present. Consequently, the low frequency peak in the spectrum gradually fades away as M_{II} increases in this region. This region has been shaded in Fig. 8. Only the part corresponding to lower M_{II} values may be excluded by the PTA bound.
- For $13.68 \lesssim \log_{10}(M_{II}/\text{GeV}) \lesssim 13.70$, the strings enter the horizon after t_{eq} and the significant low frequency peak in the gravity wave spectrum is absent. Consequently, there is no restriction from the PTA experiment.

- For $\log_{10}(M_{II}/\text{GeV}) \gtrsim 13.70$, the strings never enter the horizon and thus again no restriction arises.

9 Phase Transition after Inflation

The phase transition occurs during inflaton oscillations or even after reheating if M_{II} does not satisfy the inequality in Eq. (8.2), i.e. if $M_{II} \lesssim 4.36 \times 10^{12}$ GeV. The PTA bound is certainly well satisfied in this case. Strings produced after the end of inflation always remain inside the post-inflationary horizon. It is interesting to note that the causality criterion forbids the inter-string distance to be bigger than the horizon size. Long strings reach the scaling solution quickly with one string segment per horizon and start generating loops almost instantaneously.

At the beginning of inflaton oscillations, the corrections to the mass-squared of the field χ_{II} are not dominated by the temperature corrections from the “new” radiation, but by the Hubble parameter H_ϕ from the energy density $\rho_\phi(t)$ of the oscillating inflaton [85]. Assuming that these oscillations are quadratic, we have (for a review see Ref. [86])

$$\rho_\phi(t) = \rho_e \left(\frac{t}{\tau} \right)^{-2} \exp[-\Gamma_\phi(t - \tau)], \quad (9.1)$$

where $\Gamma_\phi \simeq 2.8$ GeV is the inflaton decay width. Therefore, right after the end of inflation, the correction to the χ_{II} mass-squared term is

$$\frac{1}{2} \sigma \left(\frac{H_\phi}{2\pi} \right)^2 \chi_{II}^2, \quad (9.2)$$

where $H_\phi = \sqrt{\rho_\phi/3m_{\text{Pl}}^2}$ and the corresponding Hawking temperature is $T_H = H_\phi/2\pi$. Here, we set $\sigma = 1$ so that continuity of the correction between the inflationary and the oscillatory era is guaranteed. Using the correction in Eq. (9.2) and following the analysis of Sec. 6, one can then calculate the value of χ_{II} at the minima of the potential with the mean value of $\phi^2 \simeq M^2$, since ϕ oscillates about M with an amplitude smaller than M . The potential difference ΔV between the local maximum at $\chi_{II} = 0$ and these minima, as well as the effective mass m_{eff} of χ_{II} at the minima are also estimated. The Ginzburg criterion for this case then takes the form:

$$\frac{4\pi}{3} m_{\text{eff}}^{-3} \Delta V > T_H \Rightarrow \beta_{II}^2 M^2 > \left(\frac{72a_{II}^2}{\pi^2} + \sigma \right) T_H^2. \quad (9.3)$$

The value of T_H (and thus ρ_ϕ) at which the phase transition takes place for given M_{II} can be calculated by saturating this inequality.

The new radiation energy density ρ_r is given by (for a review see Ref. [86])

$$\rho_r(t) = \rho_e \left(\frac{t}{\tau} \right)^{-8/3} \int_\tau^t \left(\frac{t'}{\tau} \right)^{2/3} \exp[-\Gamma_\phi(t' - \tau)] dt', \quad (9.4)$$

and its temperature T can be found from $\rho_r = (\pi^2/30)g_*T^4$. As it turns out, T soon becomes larger than T_H and dominates the correction to the mass-squared term of χ_{II} , which takes the form $(1/2)\sigma'T^2\chi_{II}^2$. Here σ' is, in principle, different from σ , but for simplicity we take it again equal to unity. Needless to say that, in m_{eff}^2 and ΔV , T_H and σ should be replaced by T and σ' respectively, and ϕ^2 by M^2 . The Ginzburg criterion is then as in Eq. (9.3) with T_H replaced by T and σ replaced by σ' . The temperature T of the new radiation at which the transition takes place for given M_{II} is again calculated by saturating the Ginzburg criterion. It is important to note that there is continuity of the χ_{II} mass-squared correction between the regimes where this correction is dominated by T_H or T . The latter regime smoothly extends even to the period after reheating.

$\frac{V_0^{1/4}}{10^{16}\text{GeV}}$	$H_\phi(10^{12}\text{ GeV})$ at $T_H = T$	$T(10^{12}\text{ GeV})$ at $T_H = T$	$\log_{10}(M_{II}/\text{GeV})$ at		$t(10^{-12}\text{ GeV}^{-1})$ at	
			end of inflation	$T_H = T$	end of inflation	$T_H = T$
1.51	8.92	1.42	12.63	12.57	1.38	1.49
1.59	9.06	1.44	12.64	12.58	1.32	1.42
1.66	9.16	1.46	12.64	12.58	1.26	1.37
1.74	9.23	1.47	12.65	12.58	1.22	1.33
1.82	9.27	1.48	12.65	12.59	1.18	1.29

Table 8: Hubble parameter H_ϕ from the oscillating inflaton and the temperature of the new radiation with $T_H = T$ for various $V_0^{1/4}$ values corresponding to successful inflation. We also show the breaking scale M_{II} and the cosmic time t at the end of inflation and at $T_H = T$ for comparison. After the cosmic time at $T_H = T$, the new radiation dominates over the Hawking temperature T_H from field oscillations.

In order to find the limiting value of M_{II} which separates the two regimes where the correction to the χ_{II} mass-squared is dominated by the oscillating inflaton or the new radiation, we compare T_H and T calculated by using Eq. (9.1) and Eq. (9.4) respectively. We then find the cosmic time at which these two temperatures coincide and their common value. Saturating the Ginzburg criterion in Eq. (9.3), we finally estimate the limiting value of M_{II} . The value of the Hubble parameter H_ϕ from inflaton oscillations and the cosmic temperature for $T_H = T$ are given in Table 8 for successful inflation. We also provide in this table the breaking scale M_{II} and the cosmic time t at the end of inflation and at $T_H = T$ for comparison. After the cosmic time at which $T_H = T$, the temperature of the new radiation starts dominating over the Hawking temperature T_H . The variation of T_H and T with the cosmic time t is shown in Fig. 9 for $V_0^{1/4} = 1.66 \times 10^{16}\text{ GeV}$.

Loops that are produced during any phase transition occurring within the era of inflaton oscillations decay much earlier than the equidensity time t_{eq} . Indeed, a phase transition taking place at the reheat time $t_r \simeq 0.36\text{ GeV}^{-1}$ corresponds to a breaking scale around $M_{II} \simeq 2.34 \times 10^9\text{ GeV}$. The lifetime of the loops of size $\sim t_r/10$ generated at this transition is $6.43 \times 10^{15}\text{ GeV}^{-1}$ and thus these loops contribute to the plateau in the gravity wave spectrum. During radiation dominance, a loop produced at cosmic temperature T and time t decays at t_{eq} if

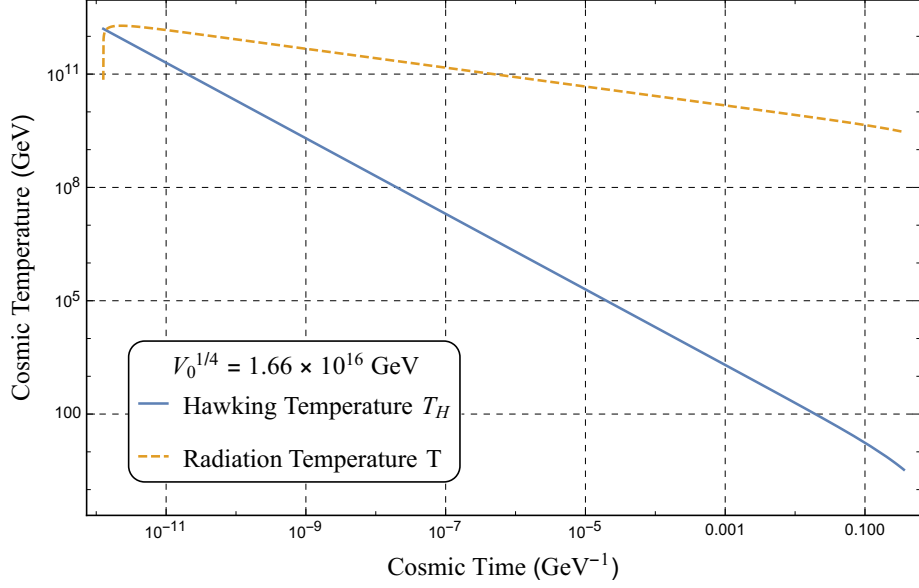


Figure 9: Hawking Temperature $T_H = H_\phi/2\pi$, with H_ϕ being the Hubble parameter from the energy density ρ_ϕ of the inflaton oscillations, and new radiation temperature T versus cosmic time for successful inflation with $V_0^{1/4} = 1.66 \times 10^{16}$ GeV. The new radiation temperature T starts dominating over T_H after cosmic time 1.37×10^{-12} GeV $^{-1}$, and inflation ends at $\tau = 1.26 \times 10^{-12}$ GeV $^{-1}$.

$t \simeq 10(\Gamma G\mu)t_{eq}$, where t and $G\mu$ are estimated from Eqs. (8.5) and (8.4), respectively. The minimum value of the symmetry breaking scale M_{II} for which the loops generated during the corresponding phase transition in a radiation dominated universe contribute to the sharp peak in the gravity wave spectrum can then be found from the Ginzburg criterion and turns out to be 2.6×10^4 GeV.

10 Conclusions

We have explored in this paper the appearance and subsequent evolution of topologically stable magnetic monopoles and cosmic strings in realistic non-supersymmetric SO(10) and E_6 GUTs. As an important first step we perform a comprehensive study of GUT symmetry breaking with two intermediate scales that is compatible with gauge coupling unification and proton decay limits. In turn, this allows us to identify the monopoles and strings associated with the GUT and intermediate scale symmetry breakings. Topological defects with intermediate scales are of special interest and, to keep things realistic, we explore their evolution within the context of an inflationary universe. We highlight models which predict the presence of an observable number density of primordial monopoles with mass $\sim 10^{13} - 10^{14}$ GeV and cosmic strings with the string tension parameter $G\mu \sim 10^{-11} - 10^{-10}$ that have survived an inflationary epoch. The impact of inflation on the stochastic gravitational background radiation emitted by strings

is also discussed. Finally, we note that $G\mu$ values lying in a wide range $\sim 10^{-10} - 10^{-20}$ will be probed by a variety of proposed experiments including LISA [87, 88], SKA [89, 90], BBO [91, 92], and ET [93].

11 Acknowledgment

The work of J.C. and R.M. is supported by the Science and Engineering Research Board, Government of India, under the agreements SERB/PHY/2016348 (Early Career Research Award) and SERB/PHY/2019501 (MATRICS). The work of G.L. and Q.S. is supported by the Hellenic Foundation for Research and Innovation (H.F.R.I.) under the “First Call for H.F.R.I. Research Projects to support Faculty Members and Researchers and the procurement of high-cost research equipment grant” (Project Number:2251). Q.S. thanks Nefer Vedat Şenoğuz for a useful discussion.

Appendix: RGEs for the Two Breaking Chains of $SO(10)$

A.1 The RGEs and β -coefficients for the Breaking Chain in Sec. 3.1

From M_{II} to M_I :

$$\mu \frac{dg_{2L}}{d\mu} = \frac{1}{(4\pi)^2} (-3g_{2L}^3) + \frac{1}{(4\pi)^4} \left(8g_{2L}^5 + 12g_{2L}^3 g_{3C}^2 + \frac{3g_{2L}^3}{2} g_{XX}^2 + g_{2L}^3 g_{RR}^2 + g_{2L}^3 g_{RX}^2 + \frac{3g_{2L}^3}{2} g_{XR}^2 \right),$$

$$\mu \frac{dg_{3C}}{d\mu} = \frac{1}{(4\pi)^2} (-7g_{3C}^3) + \frac{1}{(4\pi)^4} \left(\frac{9g_{2L}^2}{2} g_{3C}^3 - 26g_{3C}^5 + \frac{g_{3C}^3}{2} g_{XX}^2 + \frac{3g_{3C}^3}{2} g_{RR}^2 + \frac{3g_{3C}^3}{2} g_{RX}^2 + \frac{g_{3C}^3}{2} g_{XR}^2 \right),$$

$$\begin{aligned} \mu \frac{dg_{RR}}{d\mu} = & \frac{1}{(4\pi)^2} \left(\frac{53}{12} g_{RR}^3 - \frac{\sqrt{6}}{12} g_{XR} g_{RR}^2 + \frac{53}{12} g_{RR} g_{RX}^2 + \frac{33}{8} g_{RR} g_{XR}^2 \right. \\ & \left. - \frac{g_{XX}}{24} g_{RR} \sqrt{6} g_{RX} + \frac{33}{8} g_{XX} g_{RX} g_{XR} - \frac{g_{XR}}{24} \sqrt{6} g_{RX}^2 \right) \\ & + \frac{1}{(4\pi)^4} \left(3g_{2L}^2 g_{RR}^3 + 12g_{3C}^2 g_{RR}^3 + \frac{15}{8} g_{XX}^2 g_{RR}^3 + \frac{17}{4} g_{RR}^5 \right. \\ & \left. + \frac{17}{2} g_{RR}^3 g_{RX}^2 + \frac{17}{4} g_{RR} g_{RX}^4 + 3g_{2L}^2 g_{RR} g_{RX}^2 + 12g_{3C}^2 g_{RR} g_{RX}^2 \right) \end{aligned}$$

$$\begin{aligned}
& + 4g_{3C}^2 g_{RR} g_{XR}^2 + \frac{45}{4} g_{RR}^3 g_{XR}^2 + \frac{65}{16} g_{RR} g_{XR}^4 - \frac{\sqrt{6}}{2} g_{XR} g_{RR}^4 \\
& - \frac{3\sqrt{6}}{4} g_{RR}^2 g_{XR}^3 - \frac{\sqrt{6}}{8} g_{XR} g_{RR}^4 - \frac{3\sqrt{6}}{16} g_{RX}^2 g_{XR}^3 + \frac{9}{2} g_{RR} g_{2L}^2 g_{XR}^2 \\
& + \frac{45}{8} g_{RR} g_{XX}^2 g_{RX}^2 + \frac{45}{8} g_{XX} g_{RX}^3 g_{XR} + \frac{15}{2} g_{RR} g_{RX}^2 g_{XR}^2 \\
& + 4g_{3C}^2 g_{XX} g_{RX} g_{XR} + \frac{65}{16} g_{XX}^3 g_{RX} g_{XR} + \frac{65}{16} g_{RR} g_{XX}^2 g_{XR}^2 \\
& + \frac{65}{16} g_{XX} g_{RX} g_{XR}^3 - \frac{9\sqrt{6}}{16} g_{XX}^2 g_{RX}^2 g_{XR} - \frac{3\sqrt{6}}{8} g_{XX} g_{RR} g_{RX}^3 \\
& - \frac{5\sqrt{6}}{8} g_{RR}^2 g_{RX}^2 g_{XR} + \frac{9}{2} g_{XX} g_{2L}^2 g_{RX} g_{XR} - \frac{3\sqrt{6}}{16} g_{RR} g_{XX}^3 g_{RX} \\
& - \frac{3\sqrt{6}}{8} g_{XX}^2 g_{RR}^2 g_{XR} - \frac{3\sqrt{6}}{8} g_{XX} g_{RR}^3 g_{RX} \\
& + \frac{105}{8} g_{XX} g_{RR}^2 g_{RX} g_{XR} - \frac{15\sqrt{6}}{16} g_{XX} g_{RR} g_{RX} g_{XR}^2 \Big) ,
\end{aligned}$$

$$\begin{aligned}
\mu \frac{dg_{RX}}{d\mu} = & \frac{1}{(4\pi)^2} \left(\frac{33}{8} g_{XX}^2 g_{RX} - \frac{\sqrt{6}}{12} g_{XX} g_{RX}^2 + \frac{53}{12} g_{RR}^2 g_{RX} + \frac{53}{12} g_{RX}^3 \right. \\
& \left. - \frac{\sqrt{6}}{24} g_{XX} g_{RR}^2 + \frac{33}{8} g_{XX} g_{RR} g_{XR} - \frac{\sqrt{6}}{24} g_{RR} g_{RX} g_{XR} \right) \\
& + \frac{1}{(4\pi)^4} \left(+3g_{2L}^2 g_{RX}^3 + 12g_{3C}^2 g_{RX}^3 + \frac{17g_{RR}^4}{4} g_{RX} + \frac{17}{2} g_{RR}^2 g_{RX}^3 \right. \\
& + \frac{17}{4} g_{RX}^5 + \frac{15}{8} g_{RX}^3 g_{XR}^2 + 3g_{2L}^2 g_{RR}^2 g_{RX} + 4g_{3C}^2 g_{XX}^2 g_{RX} \\
& + 12g_{3C}^2 g_{RR}^2 g_{RX} + \frac{65g_{XX}^4}{16} g_{RX} + \frac{45}{4} g_{XX}^2 g_{RX}^3 - \frac{3\sqrt{6}}{16} g_{XX}^3 g_{RR}^2 \\
& - \frac{3\sqrt{6}}{4} g_{XX}^3 g_{RX}^2 - \frac{\sqrt{6}}{8} g_{XX} g_{RR}^4 - \frac{\sqrt{6}}{2} g_{XX} g_{RX}^4 + \frac{9}{2} g_{2L}^2 g_{XX}^2 g_{RX} \\
& + \frac{15}{2} g_{XX}^2 g_{RR}^2 g_{RX} + \frac{45}{8} g_{XX} g_{RR}^3 g_{XR} + \frac{45}{8} g_{RR}^2 g_{RX} g_{XR}^2 \\
& + 4g_{3C}^2 g_{XX} g_{RR} g_{XR} + \frac{65}{16} g_{RR} g_{XX}^3 g_{XR} + \frac{65}{16} g_{XX}^2 g_{RX} g_{XR}^2 + \frac{65}{16} g_{XX} g_{RR} g_{XR}^3 \\
& - \frac{5\sqrt{6}}{8} g_{XX} g_{RR}^2 g_{RX}^2 - \frac{9}{16} g_{XX} \sqrt{6} g_{RR}^2 g_{XR}^2 - \frac{3\sqrt{6}}{8} g_{XX} g_{RX}^2 g_{XR}^2 \\
& + \frac{9}{2} g_{XX} g_{2L}^2 g_{RR} g_{XR} - \frac{3\sqrt{6}}{8} g_{RR}^3 g_{RX} g_{XR} - \frac{3\sqrt{6}}{8} g_{RR} g_{RX}^3 g_{XR} \\
& \left. - \frac{3\sqrt{6}}{16} g_{RR} g_{RX} g_{XR}^3 - \frac{15\sqrt{6}}{16} g_{RR} g_{XX}^2 g_{RX} g_{XR} + \frac{105}{8} g_{XX} g_{RR} g_{RX}^2 g_{XR} \right) ,
\end{aligned}$$

$$\begin{aligned}
\mu \frac{dg_{XR}}{d\mu} = & \frac{1}{(4\pi)^2} \left(\frac{33}{8} g_{XX}^2 g_{XR} + \frac{53}{12} g_{RR}^2 g_{XR} - \frac{\sqrt{6}}{12} g_{RR} g_{XR}^2 + \frac{33}{8} g_{XR}^3 \right. \\
& - \frac{\sqrt{6}}{24} g_{RR} g_{XX}^2 + \frac{53}{12} g_{XX} g_{RR} g_{RX} - \frac{\sqrt{6}}{24} g_{XX} g_{RX} g_{XR} \Big) \\
& + \frac{1}{(4\pi)^4} \left(\frac{9}{2} g_{2L}^2 g_{XR}^3 + 4g_{3C}^2 g_{XR}^3 + \frac{17}{4} g_{RR}^4 g_{XR} + \frac{15}{8} g_{RX}^2 g_{XR}^3 + \frac{65}{16} g_{XR}^5 \right. \\
& + 3g_{2L}^2 g_{RR}^2 g_{XR} + 4g_{3C}^2 g_{XX}^2 g_{XR} + \frac{65}{16} g_{XX}^4 g_{XR} + \frac{65}{8} g_{XX}^2 g_{XR}^3 + \frac{45}{4} g_{RR}^2 g_{XR}^3 \\
& + 12g_{3C}^2 g_{RR}^2 g_{XR} - \frac{3\sqrt{6}}{16} g_{RR} g_{XX}^4 - \frac{\sqrt{6}}{2} g_{RR}^3 g_{XR}^2 - \frac{3\sqrt{6}}{4} g_{RR} g_{XR}^4 \\
& + \frac{9}{2} g_{2L}^2 g_{XX}^2 g_{XR} - \frac{\sqrt{6}}{8} g_{XX}^2 g_{RR}^3 + \frac{15}{2} g_{XX}^2 g_{RR}^2 g_{XR} + \frac{17}{4} g_{XX} g_{RR} g_{RX}^3 \\
& + \frac{45}{8} g_{RR} g_{XX}^3 g_{RX} + \frac{45}{8} g_{XX}^2 g_{RX}^2 g_{XR} + \frac{17}{4} g_{XX} g_{RR}^3 g_{RX} + \frac{17}{4} g_{RR}^2 g_{RX}^2 g_{XR} \\
& + 3g_{2L}^2 g_{XX} g_{RR} g_{RX} + 12g_{3C}^2 g_{XX} g_{RR} g_{RX} - \frac{15\sqrt{6}}{16} g_{RR} g_{XX}^2 g_{XR}^2 \\
& - \frac{9\sqrt{6}}{16} g_{XX} g_{RX} g_{XR}^3 - \frac{9\sqrt{6}}{16} g_{XX}^3 g_{RX} g_{XR} - \frac{3\sqrt{6}}{8} g_{RR} g_{XX}^2 g_{RX}^2 \\
& - \frac{\sqrt{6}}{4} g_{RR} g_{RX}^2 g_{XR}^2 - \frac{5\sqrt{6}}{8} g_{XX} g_{RR}^2 g_{RX} g_{XR} + \frac{105}{8} g_{XX} g_{RR} g_{RX} g_{XR}^2 \\
& \left. - \frac{\sqrt{6}}{8} g_{XX} g_{RX}^3 g_{XR} \right) ,
\end{aligned}$$

$$\begin{aligned}
\mu \frac{dg_{XX}}{d\mu} = & \frac{1}{(4\pi)^2} \left(\frac{33}{8} g_{XX}^3 - \frac{\sqrt{6}}{12} g_{RX} g_{XX}^2 + \frac{53}{12} g_{XX} g_{RX}^2 + \frac{33}{8} g_{XX} g_{XR}^2 \right. \\
& - \frac{\sqrt{6}}{24} g_{XX} g_{RR} g_{XR} + \frac{53}{12} g_{RR} g_{RX} g_{XR} - \frac{\sqrt{6}}{24} g_{RX} g_{XR}^2 \Big) \\
& + \frac{1}{(4\pi)^4} \left(\frac{9}{2} g_{2L}^2 g_{XX}^3 + 4g_{3C}^2 g_{XX}^3 + \frac{65}{16} g_{XX}^5 + \frac{15}{8} g_{XX}^3 g_{RR}^2 \right. \\
& + \frac{45}{4} g_{XX}^3 g_{RX}^2 + \frac{17}{4} g_{XX} g_{RX}^4 + 3g_{2L}^2 g_{XX} g_{RX}^2 \\
& + 12g_{3C}^2 g_{XX} g_{RX}^2 + 4g_{3C}^2 g_{XX} g_{XR}^2 + \frac{65}{8} g_{XX}^3 g_{XR}^2 + \frac{65}{16} g_{XX} g_{XR}^4 \\
& - \frac{3\sqrt{6}}{4} g_{XX}^4 g_{RX} - \frac{\sqrt{6}}{2} g_{XX}^2 g_{RX}^3 - \frac{\sqrt{6}}{8} g_{RX}^3 g_{XR}^2 - \frac{3\sqrt{6}}{16} g_{RX} g_{XR}^4 \\
& + \frac{9}{2} g_{XX} g_{2L}^2 g_{XR}^2 + \frac{17}{4} g_{XX} g_{RR}^2 g_{RX}^2 + \frac{15}{2} g_{XX} g_{RX}^2 g_{XR}^2 + \frac{17}{4} g_{RR} g_{RX}^3 g_{XR} \Big)
\end{aligned}$$

$$\begin{aligned}
& + 3g_{2L}^2 g_{RR} g_{RX} g_{XR} + \frac{45}{8} g_{XX} g_{RR}^2 g_{XR}^2 + \frac{17}{4} g_{RR}^3 g_{RX} g_{XR} + \frac{45}{8} g_{RR} g_{RX} g_{XR}^3 \\
& + 12g_{3C}^2 g_{RR} g_{RX} g_{XR} - \frac{9\sqrt{6}}{16} g_{RR} g_{XX}^3 g_{XR} - \frac{15\sqrt{6}}{16} g_{XX}^2 g_{RX} g_{XR}^2 \\
& - \frac{9\sqrt{6}}{16} g_{XX} g_{RR} g_{XR}^3 - \frac{\sqrt{6}}{4} g_{RX} g_{XX}^2 g_{RR}^2 - \frac{\sqrt{6}}{8} g_{XX} g_{RR}^3 g_{XR} \\
& - \frac{3\sqrt{6}}{8} g_{RR}^2 g_{RX} g_{XR}^2 + \frac{105}{8} g_{RR} g_{XX}^2 g_{RX} g_{XR} - \frac{5\sqrt{6}}{8} g_{XX} g_{RR} g_{RX}^2 g_{XR} \Big) .
\end{aligned}$$

$$\text{From } M_I \text{ to } M_X : \quad b_{2L} = -3, \quad b_{2R} = \frac{26}{3}, \quad b_{4C} = -\frac{17}{3}, \quad b_{ij} = \begin{pmatrix} 8 & 3 & \frac{45}{2} \\ 3 & \frac{1004}{3} & \frac{1245}{2} \\ \frac{9}{2} & \frac{249}{2} & \frac{1315}{6} \end{pmatrix} .$$

A.2 The RGEs and β -coefficients for the Breaking Chain in Sec. 3.2

From M_{II} to M_I :

$$\begin{aligned}
\mu \frac{dg_{2L}}{d\mu} &= \frac{1}{(4\pi)^2} (-3g_{2L}^3) + \frac{1}{(4\pi)^4} \left(8g_{2L}^5 + 12g_{2L}^3 g_{3C}^2 + \frac{3g_{2L}^3}{2} g_{XX}^2 + g_{2L}^3 g_R^2 \right. \\
&\quad \left. + g_{2L}^3 g_{RX}^2 + \frac{3g_{2L}^3}{2} g_{XR}^2 \right) ,
\end{aligned}$$

$$\begin{aligned}
\mu \frac{dg_{3C}}{d\mu} &= \frac{1}{(4\pi)^2} (-7g_{3C}^3) + \frac{1}{(4\pi)^4} \left(\frac{9g_{2L}^2}{2} g_{3C}^3 - 26g_{3C}^5 + \frac{g_{3C}^3}{2} g_{XX}^2 + \frac{3g_{3C}^3}{2} g_R^2 \right. \\
&\quad \left. + \frac{3g_{3C}^3}{2} g_{RX}^2 + \frac{g_{3C}^3}{2} g_{XR}^2 \right) ,
\end{aligned}$$

$$\begin{aligned}
\mu \frac{dg_{RR}}{d\mu} &= \frac{1}{(4\pi)^2} \left(\frac{14g_{RR}^3}{3} - \frac{\sqrt{6}}{3} g_{XR} g_{RR}^2 + \frac{14}{3} g_{RR} g_{RX}^2 + \frac{9}{2} g_{RR} g_{XR}^2 \right. \\
&\quad \left. - \frac{g_{XX}}{6} g_{RR} \sqrt{6} g_{RX} + \frac{9}{2} g_{XX} g_{RX} g_{XR} - \frac{g_{XR}}{6} \sqrt{6} g_{RX}^2 \right) \\
&+ \frac{1}{(4\pi)^4} \left(3g_{2L}^2 g_{RR}^3 + 12g_{3C}^2 g_{RR}^3 + \frac{15}{2} g_{XX}^2 g_{RR}^3 + 8g_{RR}^5 + 16g_{RR}^3 g_{RX}^2 \right. \\
&+ 45g_{RR}^3 g_{XR}^2 + 8g_{RR} g_{RX}^4 - 8\sqrt{6} g_{RR}^4 g_{XR} - 12\sqrt{6} g_{RR}^2 g_{XR}^3 \\
&+ \frac{25}{2} g_{RR} g_{XR}^4 - 2\sqrt{6} g_{RX}^4 g_{XR} - 3\sqrt{6} g_{RX}^2 g_{XR}^3 + 3g_{2L}^2 g_{RR} g_{RX}^2 \\
&+ \frac{9}{2} g_{RR} g_{2L}^2 g_{XR}^2 + 12g_{3C}^2 g_{RR} g_{RX}^2 + 4g_{3C}^2 g_{RR} g_{XR}^2 + 30g_{RR} g_{RX}^2 g_{XR}^2 \Big)
\end{aligned}$$

$$\begin{aligned}
& + \frac{25g_{XX}^3}{2}g_{RX}g_{XR} + \frac{25}{2}g_{RR}g_{XX}^2g_{XR}^2 + \frac{45}{2}g_{XX}g_{RX}^3g_{XR} \\
& + \frac{25}{2}g_{XX}g_{RX}g_{XR}^3 + \frac{45}{2}g_{RR}g_{XX}^2g_{RX}^2 - 9\sqrt{6}g_{XX}^2g_{RX}^2g_{XR} \\
& - 6\sqrt{6}g_{XX}g_{RR}g_{RX}^3 - 10\sqrt{6}g_{RR}^2g_{RX}^2g_{XR} + 4g_{3C}^2g_{XX}g_{RX}g_{XR} \\
& - 3\sqrt{6}g_{XX}^3g_{RR}g_{RX} - 6\sqrt{6}g_{XX}^2g_{RR}^2g_{XR} - 6\sqrt{6}g_{XX}g_{RR}^3g_{RX} \\
& + \frac{9}{2}g_{XX}g_{2L}^2g_{RX}g_{XR} + \frac{105}{2}g_{XX}g_{RR}^2g_{RX}g_{XR} - 15\sqrt{6}g_{XX}g_{RR}g_{RX}g_{XR}^2 \Big) ,
\end{aligned}$$

$$\begin{aligned}
\mu \frac{dg_{RX}}{d\mu} = & \frac{1}{(4\pi)^2} \left(\frac{9}{2}g_{XX}^2g_{RX} - \frac{\sqrt{6}}{3}g_{XX}g_{RX}^2 + \frac{14}{3}g_{RR}^2g_{RX} + \frac{14}{3}g_{RX}^3 \right. \\
& \left. - \frac{\sqrt{6}}{6}g_{XX}g_{RR}^2 + \frac{9}{2}g_{XX}g_{RR}g_{XR} - \frac{\sqrt{6}}{6}g_{RR}g_{RX}g_{XR} \right) \\
& + \frac{1}{(4\pi)^4} (3g_{2L}^2g_{RX}^3 + 12g_{3C}^2g_{RX}^3 + 45g_{XX}^2g_{RX}^3 + 8g_{RR}^4g_{RX} + 16g_{RR}^2g_{RX}^3 \\
& + 8g_{RX}^5 + \frac{15}{2}g_{RX}^3g_{XR}^2 + \frac{25g_{XX}^4}{2}g_{RX} - 3\sqrt{6}g_{XX}^3g_{RR}^2 - 12\sqrt{6}g_{XX}^3g_{RX}^2 \\
& - 2\sqrt{6}g_{XX}g_{RR}^4 - 8\sqrt{6}g_{XX}g_{RX}^4 + \frac{9}{2}g_{2L}^2g_{XX}^2g_{RX} + 3g_{2L}^2g_{RR}^2g_{RX} \\
& + 4g_{3C}^2g_{XX}^2g_{RX} + 12g_{3C}^2g_{RR}^2g_{RX} + 30g_{XX}^2g_{RR}^2g_{RX} + \frac{25}{2}g_{RR}g_{XX}^3g_{XR} \\
& + \frac{25}{2}g_{XX}^2g_{RX}g_{XR}^2 + \frac{45}{2}g_{XX}g_{RR}^3g_{XR} + \frac{25}{2}g_{XX}g_{RR}g_{XR}^3 \\
& - 10\sqrt{6}g_{XX}g_{RR}^2g_{RX}^2 - 9\sqrt{6}g_{XX}g_{RR}^2g_{XR}^2 - 6\sqrt{6}g_{XX}g_{RX}^2g_{XR}^2 \\
& + \frac{45}{2}g_{RR}^2g_{RX}g_{XR}^2 + 4g_{3C}^2g_{XX}g_{RR}g_{XR} - 6\sqrt{6}g_{RR}^3g_{RX}g_{XR} \\
& - 6\sqrt{6}g_{RR}g_{RX}^3g_{XR} - 3\sqrt{6}g_{RR}g_{RX}g_{XR}^3 + \frac{9}{2}g_{XX}g_{2L}^2g_{RR}g_{XR} \\
& \left. - 15\sqrt{6}g_{XX}^2g_{RR}g_{RX}g_{XR} + \frac{105}{2}g_{XX}g_{RR}g_{RX}^2g_{XR} \right) ,
\end{aligned}$$

$$\begin{aligned}
\mu \frac{dg_{XR}}{d\mu} = & \frac{1}{(4\pi)^2} \left(\frac{9}{2}g_{XX}^2g_{XR} + \frac{14}{3}g_{RR}^2g_{XR} - \frac{\sqrt{6}}{3}g_{RR}g_{XR}^2 + \frac{9}{2}g_{XR}^3 \right. \\
& \left. - \frac{\sqrt{6}}{6}g_{RR}g_{XX}^2 + \frac{14}{3}g_{XX}g_{RR}g_{RX} - \frac{\sqrt{6}}{6}g_{XX}g_{RX}g_{XR} \right) \\
& + \frac{1}{(4\pi)^4} \left(\frac{9g_{2L}^2}{2}g_{XR}^3 + 4g_{3C}^2g_{XR}^3 + 25g_{XX}^2g_{XR}^3 + 8g_{RR}^4g_{XR} \right. \\
& \left. + 45g_{RR}^2g_{XR}^3 + \frac{25}{2}g_{XR}^5 - 3\sqrt{6}g_{XX}^4g_{RR} + \frac{25g_{XX}^4}{2}g_{XR} - 8\sqrt{6}g_{RR}^3g_{XR}^2 \right)
\end{aligned}$$

$$\begin{aligned}
& -12\sqrt{6}g_{RR}g_{XR}^4 + \frac{15}{2}g_{RX}^2g_{XR}^3 + 3g_{2L}^2g_{RR}^2g_{XR} + 4g_{3C}^2g_{XX}^2g_{XR} \\
& -2\sqrt{6}g_{XX}^2g_{RR}^3 + 8g_{XX}g_{RR}^3g_{RX} + 8g_{XX}g_{RR}g_{RX}^3 + 8g_{RR}^2g_{RX}^2g_{XR} \\
& + \frac{9g_{2L}^2}{2}g_{XX}^2g_{XR} + 12g_{3C}^2g_{RR}^2g_{XR} + \frac{45}{2}g_{RR}g_{XX}^3g_{RX} + 30g_{XX}^2g_{RR}^2g_{XR} \\
& -9\sqrt{6}g_{XX}^3g_{RX}g_{XR} - 15\sqrt{6}g_{XX}^2g_{RR}g_{XR}^2 + \frac{45}{2}g_{XX}^2g_{RX}^2g_{XR} \\
& -9\sqrt{6}g_{XX}g_{RX}g_{XR}^3 + 3g_{2L}^2g_{XX}g_{RR}g_{RX} - 6\sqrt{6}g_{XX}^2g_{RR}g_{RX}^2 \\
& -2\sqrt{6}g_{XX}g_{RX}^3g_{XR} - 4\sqrt{6}g_{RR}g_{RX}^2g_{XR}^2 + 12g_{3C}^2g_{XX}g_{RR}g_{RX} \\
& -10\sqrt{6}g_{XX}g_{RR}^2g_{RX}g_{XR} + \frac{105}{2}g_{XX}g_{RR}g_{RX}g_{XR}^2 \Big) ,
\end{aligned}$$

$$\begin{aligned}
\mu \frac{dg_{XX}}{d\mu} = & \frac{1}{(4\pi)^2} \left(\frac{9g_{XX}^3}{2} - \frac{g_{RX}}{3}\sqrt{6}g_{XX}^2 + \frac{14}{3}g_{XX}g_{RX}^2 + \frac{9}{2}g_{XX}g_{XR}^2 \right. \\
& \left. - \frac{\sqrt{6}}{6}g_{RR}g_{XX}g_{XR} + \frac{14}{3}g_{RR}g_{RX}g_{XR} - \frac{\sqrt{6}}{6}g_{RX}g_{XR}^2 \right) \\
& + \frac{1}{(4\pi)^4} \left(\frac{9g_{2L}^2}{2}g_{XX}^3 + 4g_{3C}^2g_{XX}^3 + \frac{25g_{XX}^5}{2} + 45g_{XX}^3g_{RX}^2 \right. \\
& + 25g_{XX}^3g_{XR}^2 + 8g_{XX}g_{RX}^4 - 12\sqrt{6}g_{XX}^4g_{RX} + \frac{15}{2}g_{XX}^3g_{RR}^2 \\
& - 8\sqrt{6}g_{XX}^2g_{RX}^3 + \frac{25}{2}g_{XX}g_{XR}^4 - 3\sqrt{6}g_{RX}g_{XR}^4 + 3g_{2L}^2g_{XX}g_{RX}^2 \\
& + 4g_{3C}^2g_{XX}g_{XR}^2 + 8g_{XX}g_{RR}^2g_{RX}^2 + 8g_{RR}g_{RX}^3g_{XR} - 2\sqrt{6}g_{RX}^3g_{XR}^2 \\
& + \frac{9}{2}g_{XX}g_{2L}^2g_{XR}^2 + 12g_{3C}^2g_{XX}g_{RX}^2 + \frac{45}{2}g_{XX}g_{RR}^2g_{XR}^2 + 30g_{XX}g_{RX}^2g_{XR}^2 \\
& + 8g_{RR}^3g_{RX}g_{XR} - 9\sqrt{6}g_{XX}^3g_{RR}g_{XR} - 15\sqrt{6}g_{XX}^2g_{RX}g_{XR}^2 \\
& - 9\sqrt{6}g_{XX}g_{RR}g_{XR}^3 + \frac{45}{2}g_{RR}g_{RX}g_{XR}^3 + 3g_{2L}^2g_{RR}g_{RX}g_{XR} \\
& - 4\sqrt{6}g_{XX}^2g_{RR}^2g_{RX} - 2\sqrt{6}g_{XX}g_{RR}^3g_{XR} - 6\sqrt{6}g_{RR}^2g_{RX}g_{XR}^2 \\
& \left. + 12g_{3C}^2g_{RR}g_{RX}g_{XR} + \frac{105}{2}g_{RR}g_{XX}^2g_{RX}g_{XR} - 10\sqrt{6}g_{XX}g_{RR}g_{RX}^2g_{XR} \right) .
\end{aligned}$$

$$\text{From } M_I \text{ to } M_X : \quad b_{2L} = -3, \quad b_{2R} = \frac{8}{3}, \quad b_{4C} = -\frac{25}{3}, \quad b_{ij} = \begin{pmatrix} 8 & 3 & \frac{45}{2} \\ 3 & \frac{470}{3} & \frac{555}{2} \\ \frac{9}{2} & \frac{111}{2} & \frac{130}{3} \end{pmatrix} .$$

References

- [1] G. 't Hooft, *Magnetic Monopoles in Unified Gauge Theories*, *Nucl. Phys. B* **79** (1974) 276.
- [2] A.M. Polyakov, *Particle Spectrum in the Quantum Field Theory*, *JETP Lett.* **20** (1974) 194.
- [3] M. Daniel, G. Lazarides and Q. Shafi, *$SU(5)$ Monopoles, Magnetic Symmetry and Confinement*, *Nucl. Phys. B* **170** (1980) 156.
- [4] G. Lazarides, Q. Shafi and W. Trower, *Consequences of a Monopole With Dirac Magnetic Charge*, *Phys. Rev. Lett.* **49** (1982) 1756.
- [5] J.C. Pati and A. Salam, *Lepton Number as the Fourth Color*, *Phys. Rev. D* **10** (1974) 275.
- [6] G. Lazarides, M. Magg and Q. Shafi, *Phase Transitions and Magnetic Monopoles in $SO(10)$* , *Phys. Lett. B* **97** (1980) 87.
- [7] G. Lazarides and Q. Shafi, *Monopoles, Strings, and Necklaces in $SO(10)$ and E_6* , *JHEP* **10** (2019) 193 [[1904.06880](#)].
- [8] Q. Shafi and C. Wetterich, *Magnetic Monopoles in Grand Unified and Kaluza-Klein Theories*, *NATO Sci. Ser. B* **111** (1984) 47.
- [9] G. Lazarides, C. Panagiotakopoulos and Q. Shafi, *Magnetic Monopoles From Superstring Models*, *Phys. Rev. Lett.* **58** (1987) 1707.
- [10] G. Lazarides, Q. Shafi and T. Tomaras, *Nonexistence of Spherically Symmetric Monopole Solutions in the Three Generation Superstring Model*, *Phys. Rev. D* **39** (1989) 1239.
- [11] T.W. Kephart, C.-A. Lee and Q. Shafi, *Family unification, exotic states and light magnetic monopoles*, *JHEP* **01** (2007) 088 [[hep-ph/0602055](#)].
- [12] T.W. Kephart, G.K. Leontaris and Q. Shafi, *Magnetic Monopoles and Free Fractionally Charged States at Accelerators and in Cosmic Rays*, *JHEP* **10** (2017) 176 [[1707.08067](#)].
- [13] T.W.B. Kibble, G. Lazarides and Q. Shafi, *Strings in $SO(10)$* , *Phys. Lett. B* **113** (1982) 237.
- [14] C. Dvorkin, M. Wyman and W. Hu, *Cosmic String Constraints from WMAP and the South Pole Telescope*, *Phys. Rev. D* **84** (2011) 123519 [[1109.4947](#)].
- [15] PLANCK collaboration, *Planck 2013 results. XXV. Searches for cosmic strings and other topological defects*, *Astron. Astrophys.* **571** (2014) A25 [[1303.5085](#)].
- [16] L. Lentati et al., *European Pulsar Timing Array Limits On An Isotropic Stochastic Gravitational-Wave Background*, *Mon. Not. Roy. Astron. Soc.* **453** (2015) 2576 [[1504.03692](#)].
- [17] R. Shannon et al., *Gravitational waves from binary supermassive black holes missing in pulsar observations*, *Science* **349** (2015) 1522 [[1509.07320](#)].
- [18] J.J. Blanco-Pillado, K.D. Olum and X. Siemens, *New limits on cosmic strings from gravitational wave observation*, *Phys. Lett. B* **778** (2018) 392 [[1709.02434](#)].
- [19] NANOGrav collaboration, *The NANOGrav 11-year Data Set: Pulsar-timing Constraints On The Stochastic Gravitational-wave Background*, *Astrophys. J.* **859** (2018) 47 [[1801.02617](#)].

- [20] W. Buchmuller, V. Domcke, H. Murayama and K. Schmitz, *Probing the scale of grand unification with gravitational waves*, *Phys. Lett. B* **809** (2020) 135764 [[1912.03695](#)].
- [21] NANOGrav collaboration, *The NANOGrav 12.5-year Data Set: Search For An Isotropic Stochastic Gravitational-Wave Background*, [2009.04496](#).
- [22] J. Ellis and M. Lewicki, *Cosmic String Interpretation of NANOGrav Pulsar Timing Data*, [2009.06555](#).
- [23] W. Buchmuller, V. Domcke and K. Schmitz, *From NANOGrav to LIGO with metastable cosmic strings*, [2009.10649](#).
- [24] NANOGrav collaboration, *Astrophysics Milestones For Pulsar Timing Array Gravitational Wave Detection*, [2010.11950](#).
- [25] Q. Shafi and A. Vilenkin, *Inflation with $SU(5)$* , *Phys. Rev. Lett.* **52** (1984) 691.
- [26] Q. Shafi and V.N. Şenoğuz, *Coleman-Weinberg potential in good agreement with WMAP*, *Phys. Rev. D* **73** (2006) 127301 [[astro-ph/0603830](#)].
- [27] D.J. Gross and F. Wilczek, *Ultraviolet behavior of non-abelian gauge theories*, *Phys. Rev. Lett.* **30** (1973) 1343.
- [28] W.E. Caswell, *Asymptotic Behavior of Nonabelian Gauge Theories to Two Loop Order*, *Phys. Rev. Lett.* **33** (1974) 244.
- [29] D.R.T. Jones, *Two Loop Diagrams in Yang-Mills Theory*, *Nucl. Phys. B* **75** (1974) 531.
- [30] D.R.T. Jones, *The Two Loop β Function for a $G_1 \times G_2$ Gauge Theory*, *Phys. Rev. D* **25** (1982) 581.
- [31] M.E. Machacek and M.T. Vaughn, *Two Loop Renormalization Group Equations in a General Quantum Field Theory. 1. Wave Function Renormalization*, *Nucl. Phys. B* **222** (1983) 83.
- [32] M.E. Machacek and M.T. Vaughn, *Two Loop Renormalization Group Equations in a General Quantum Field Theory. 2. Yukawa Couplings*, *Nucl. Phys. B* **236** (1984) 221.
- [33] M.E. Machacek and M.T. Vaughn, *Two Loop Renormalization Group Equations in a General Quantum Field Theory. 3. Scalar Quartic Couplings*, *Nucl. Phys. B* **249** (1985) 70.
- [34] B. Holdom, *Two $U(1)$'s and Epsilon Charge Shifts*, *Phys. Lett. B* **166** (1986) 196.
- [35] F. del Aguila, G.D. Coughlan and M. Quiros, *Gauge Coupling Renormalization With Several $U(1)$ Factors*, *Nucl. Phys. B* **307** (1988) 633.
- [36] L. Lavoura, *On the renormalization group analysis of gauge groups containing $U(1) \times U(1)$ factors*, *Phys. Rev. D* **48** (1993) 2356.
- [37] F. del Aguila, M. Masip and M. Perez-Victoria, *Physical parameters and renormalization of $U(1)^a \times U(1)^b$ models*, *Nucl. Phys. B* **456** (1995) 531 [[hep-ph/9507455](#)].
- [38] S. Bertolini, L. Di Luzio and M. Malinsky, *Intermediate mass scales in the non-supersymmetric $SO(10)$ grand unification: A Reappraisal*, *Phys. Rev. D* **80** (2009) 015013 [[0903.4049](#)].
- [39] J. Chakraborty and A. Raychaudhuri, *GUTs with dim-5 interactions: Gauge Unification and Intermediate Scales*, *Phys. Rev. D* **81** (2010) 055004 [[0909.3905](#)].

- [40] R.M. Fonseca, M. Malinský and F. Staub, *Renormalization group equations and matching in a general quantum field theory with kinetic mixing*, *Phys. Lett. B* **726** (2013) 882 [[1308.1674](#)].
- [41] J. Chakrabortty, R. Maji, S.K. Patra, T. Srivastava and S. Mohanty, *Roadmap of left-right models based on GUTs*, *Phys. Rev. D* **97** (2018) 095010 [[1711.11391](#)].
- [42] S. Weinberg, *Effective gauge theories*, *Phys. Lett. B* **91** (1980) 51.
- [43] L.J. Hall, *Grand Unification of Effective Gauge Theories*, *Nucl. Phys. B* **178** (1981) 75.
- [44] S. Bertolini, L. Di Luzio and M. Malinsky, *Light color octet scalars in the minimal $SO(10)$ grand unification*, *Phys. Rev. D* **87** (2013) 085020 [[1302.3401](#)].
- [45] J. Chakrabortty, R. Maji and S.F. King, *Unification, Proton Decay and Topological Defects in non-SUSY GUTs with Thresholds*, *Phys. Rev. D* **99** (2019) 095008 [[1901.05867](#)].
- [46] T. Bandyopadhyay and R. Maji, *The E_6 route to multicomponent dark matter*, [1911.13298](#).
- [47] T.W.B. Kibble, G. Lazarides and Q. Shafi, *Walls Bounded by Strings*, *Phys. Rev. D* **26** (1982) 435.
- [48] T. Ohlsson, M. Pernow and E. Sönnerlind, *Realizing unification in $SO(10)$ models with one intermediate breaking scale*, [2006.13936](#).
- [49] PARTICLE DATA GROUP collaboration, *Review of Particle Physics*, *Phys. Rev. D* **98** (2018) 030001.
- [50] S. Weinberg, *Baryon and Lepton Nonconserving Processes*, *Phys. Rev. Lett.* **43** (1979) 1566.
- [51] F. Wilczek and A. Zee, *Operator Analysis of Nucleon Decay*, *Phys. Rev. Lett.* **43** (1979) 1571.
- [52] S. Weinberg, *Varieties of Baryon and Lepton Nonconservation*, *Phys. Rev. D* **22** (1980) 1694.
- [53] L.F. Abbott and M.B. Wise, *The Effective Hamiltonian for Nucleon Decay*, *Phys. Rev. D* **22** (1980) 2208.
- [54] W. Lucha, *Proton Decay in Grand Unified Theories*, *Fortsch. Phys.* **33** (1985) 547.
- [55] P. Fileviez Pérez, *Fermion mixings versus $d = 6$ proton decay*, *Phys. Lett. B* **595** (2004) 476 [[hep-ph/0403286](#)].
- [56] P. Nath and P. Fileviez Pérez, *Proton stability in grand unified theories, in strings and in branes*, *Phys. Rept.* **441** (2007) 191 [[hep-ph/0601023](#)].
- [57] A.J. Buras, J.R. Ellis, M.K. Gaillard and D.V. Nanopoulos, *Aspects of the Grand Unification of Strong, Weak and Electromagnetic Interactions*, *Nucl. Phys. B* **135** (1978) 66.
- [58] J.T. Goldman and D.A. Ross, *How Accurately Can We Estimate the Proton Lifetime in an $SU(5)$ Grand Unified Model?*, *Nucl. Phys. B* **171** (1980) 273.
- [59] W.E. Caswell, J. Milutinović and G. Senjanović, *Predictions of Left-right Symmetric Grand Unified Theories*, *Phys. Rev. D* **26** (1982) 161.
- [60] M. Daniel and J. Peñarrocha, *Next to leading enhancement factor for proton decay in $SU(5)$* , *Phys. Lett. B* **127** (1983) 219.

- [61] L.E. Ibáñez and C. Muñoz, *Enhancement Factors for Supersymmetric Proton Decay in the Wess-Zumino Gauge*, *Nucl. Phys. B* **245** (1984) 425.
- [62] C. Muñoz, *Enhancement factors for supersymmetric proton decay in $SU(5)$ and $SO(10)$ with superfield techniques*, *Phys. Lett. B* **177** (1986) 55.
- [63] T. Nihei and J. Arafune, *The Two loop long range effect on the proton decay effective Lagrangian*, *Prog. Theor. Phys.* **93** (1995) 665 [[hep-ph/9412325](#)].
- [64] Y. Aoki, T. Izubuchi, E. Shintani and A. Soni, *Improved lattice computation of proton decay matrix elements*, *Phys. Rev. D* **96** (2017) 014506 [[1705.01338](#)].
- [65] SUPER-KAMIOKANDE collaboration, *Search for proton decay via $p \rightarrow e^+ \pi^0$ and $p \rightarrow \mu^+ \pi^0$ in 0.31 megaton-years exposure of the Super-Kamiokande water Cherenkov detector*, *Phys. Rev. D* **95** (2017) 012004 [[1610.03597](#)].
- [66] SUPER-KAMIOKANDE collaboration, *Review of Nucleon Decay Searches at Super-Kamiokande*, in *Proceedings, 51st Rencontres de Moriond on Electroweak Interactions and Unified Theories: La Thuile, Italy, March 12-19, 2016*, pp. 437–444, 2016 [[1605.03235](#)].
- [67] HYPER-KAMIOKANDE PROTO collaboration, *The Hyper-Kamiokande Experiment*, in *Proceedings, Prospects in Neutrino Physics (NuPhys2016): London, UK, December 12-14, 2016, 2017* [[1705.00306](#)].
- [68] PLANCK collaboration, *Planck 2018 results. X. Constraints on inflation*, *Astron. Astrophys.* **641** (2020) A10 [[1807.06211](#)].
- [69] G. Lazarides and Q. Shafi, *Extended Structures at Intermediate Scales in an Inflationary Cosmology*, *Phys. Lett. B* **148** (1984) 35–38.
- [70] D.H. Lyth and A.R. Liddle, *The primordial density perturbation: Cosmology, inflation and the origin of structure*, Cambridge University Press (2009).
- [71] A.R. Liddle and S.M. Leach, *How long before the end of inflation were observable perturbations produced?*, *Phys. Rev. D* **68** (2003) 103503 [[astro-ph/0305263](#)].
- [72] V.N. Şenoğuz and Q. Shafi, *Primordial monopoles, proton decay, gravity waves and GUT inflation*, *Phys. Lett. B* **752** (2016) 169 [[1510.04442](#)].
- [73] N. Okada, M.U. Rehman and Q. Shafi, *Tensor to Scalar Ratio in Non-Minimal ϕ^4 Inflation*, *Phys. Rev. D* **82** (2010) 043502 [[1005.5161](#)].
- [74] N. Bostan, O. Güleriyüz and V.N. Şenoğuz, *Inflationary predictions of double-well, Coleman-Weinberg, and hilltop potentials with non-minimal coupling*, *JCAP* **05** (2018) 046 [[1802.04160](#)].
- [75] V.L. Ginzburg, *Some Remarks on Phase Transitions of the Second Kind and the Microscopic theory of Ferroelectric Materials*, *Soviet Phys. Solid State* **2** (1961) 1824.
- [76] MACRO collaboration, *Final results of magnetic monopole searches with the MACRO experiment*, *Eur. Phys. J. C* **25** (2002) 511 [[hep-ex/0207020](#)].
- [77] E.W. Kolb and M.S. Turner, *The Early Universe*, *Front. Phys.* **69** (1990) 1.

- [78] N. Bevis, M. Hindmarsh, M. Kunz and J. Urrestilla, *CMB power spectrum contribution from cosmic strings using field-evolution simulations of the Abelian Higgs model*, *Phys. Rev. D* **75** (2007) 065015 [[astro-ph/0605018](#)].
- [79] N. Bevis, M. Hindmarsh, M. Kunz and J. Urrestilla, *CMB polarization power spectra contributions from a network of cosmic strings*, *Phys. Rev. D* **76** (2007) 043005 [[0704.3800](#)].
- [80] N. Bevis, M. Hindmarsh, M. Kunz and J. Urrestilla, *Fitting CMB data with cosmic strings and inflation*, *Phys. Rev. Lett.* **100** (2008) 021301 [[astro-ph/0702223](#)].
- [81] J.J. Blanco-Pillado, K.D. Olum and B. Shlaer, *The number of cosmic string loops*, *Phys. Rev. D* **89** (2014) 023512 [[1309.6637](#)].
- [82] J.J. Blanco-Pillado and K.D. Olum, *Stochastic gravitational wave background from smoothed cosmic string loops*, *Phys. Rev. D* **96** (2017) 104046 [[1709.02693](#)].
- [83] A. Vilenkin and E.S. Shellard, *Cosmic Strings and Other Topological Defects*, Cambridge University Press (2000).
- [84] L. Sousa, P.P. Avelino and G.S. Guedes, *Full analytical approximation to the stochastic gravitational wave background generated by cosmic string networks*, *Phys. Rev. D* **101** (2020) 103508 [[2002.01079](#)].
- [85] M. Dine, W. Fischler and D. Nemeschansky, *Solution of the Entropy Crisis of Supersymmetric Theories*, *Phys. Lett. B* **136** (1984) 169.
- [86] G. Lazarides, *Inflationary cosmology*, *Lect. Notes Phys.* **592** (2002) 351 [[hep-ph/0111328](#)].
- [87] N. Bartolo et al., *Science with the space-based interferometer LISA. IV: Probing inflation with gravitational waves*, *JCAP* **12** (2016) 026 [[1610.06481](#)].
- [88] P. Amaro-Seoane, H. Audley, S. Babak, J. Baker, E. Barausse, P. Bender et al., *Laser interferometer space antenna*, [1702.00786](#).
- [89] P.E. Dewdney, P.J. Hall, R.T. Schilizzi and T.J.L.W. Lazio, *The square kilometre array*, *Proceedings of the IEEE* **97** (2009) 1482.
- [90] G. Janssen et al., *Gravitational wave astronomy with the SKA*, *PoS AASKA14* (2015) 037 [[1501.00127](#)].
- [91] J. Crowder and N.J. Cornish, *Beyond LISA: Exploring future gravitational wave missions*, *Phys. Rev. D* **72** (2005) 083005 [[gr-qc/0506015](#)].
- [92] V. Corbin and N.J. Cornish, *Detecting the cosmic gravitational wave background with the big bang observer*, *Class. Quant. Grav.* **23** (2006) 2435 [[gr-qc/0512039](#)].
- [93] G. Mentasti and M. Peloso, *ET sensitivity to the anisotropic Stochastic Gravitational Wave Background*, [2010.00486](#).